Impacts of an unknown daytime nitrous acid source on its daytime concentration and budget, as well as those of hydroxyl, hydroperoxyl, and organic peroxy radicals, in the coastal regions of China

Yujia Tang[1,2], Junling An[1*], Feng Wang[1,2,3], Ying Li[1], Yu Qu[1], Yong Chen[1], Jian Lin[1,2]

[1]State Key Laboratory of Atmospheric Boundary Layer Physics and Atmospheric Chemistry (LAPC), Institute of Atmospheric Physics (IAP), Chinese Academy of Sciences, Beijing 100029, China

[2]University of the Chinese Academy of Sciences, Beijing 100049, China

[3]Anhui Meteorological Bureau, Hefei 230061, China

[*]Corresponding author: anjl@mail.iap.ac.cn

Abstract

Many field experiments have found high nitrous acid (HONO) mixing ratios in both urban and rural areas during daytime, but these high daytime HONO mixing ratios cannot be explained well by gas-phase production, suggesting that an unknown daytime HONO source ($P_{unknown}$) could exist. The formula $P_{unknown} \approx 19.60[NO_2] \cdot J(NO_2)$ was obtained using observed data from 13 field experiments across the globe. The additional HONO sources [i.e. the $P_{unknown}$, HONO emissions, and nighttime hydrolysis conversion of nitrogen dioxide (NO_2) on aerosols] were coupled into the WRF-Chem model (Weather Research and Forecasting model coupled with Chemistry) to assess the $P_{unknown}$ impacts on the concentrations and budgets of HONO and peroxy (hydroxyl, hydroperoxyl, and organic peroxy) radicals (RO_x) (= OH + HO_2 + RO_2) in the coastal regions of China.

Results indicated that the additional HONO sources produced a significant improvement in HONO and OH simulations, particularly in the daytime. Elevated daytime average $P_{unknown}$ values were found in the coastal regions of China, with a maximum of 2.5 ppb h^{-1} in the Beijing–Tianjin–Hebei region. The $P_{unknown}$ produced a 60%–250% increase of OH, HO_2 and RO_2 near the ground in the major cities of the coastal regions of China, and a 5–48% increase of OH, HO_2 and RO_2 in the daytime meridional-mean mixing ratios within 1000 m above the ground. When the additional HONO sources were included, the photolysis of HONO was the second source in the OH production rate in Beijing, Shanghai and Guangzhou before 10:00 LST with a maximum of 3.72 [3.06 due to the $P_{unknown}$] ppb h^{-1} in Beijing, whereas the reaction of HO_2 + NO (nitric oxide) was dominated after 10:00 LST with a maximum of 9.38 [7.23] ppb h^{-1} in Beijing. The whole RO_x cycle was accelerated by the additional HONO sources, especially the $P_{unknown}$. The daytime average OH production rate was enhanced by 0.67 [0.64] to 4.32 [3.86] ppb h^{-1} via the reaction of HO_2 + NO, and by 0.49 [0.47] to 1.86 [1.86] ppb h^{-1} via the photolysis of HONO, and the OH daytime average loss rate was enhanced by 0.58 [0.55] to 2.03 [1.92] ppb h^{-1} via the reaction of OH + NO_2 and by 0.31 [0.28] to 1.78 [1.64] ppb h^{-1} via the reaction of OH + CO (carbon monoxide) in Beijing, Shanghai and Guangzhou. Similarly, the additional HONO sources produced an increase of 0.31 [0.28] to 1.78 [1.64] ppb h^{-1} via the reaction of OH + CO and 0.10 [0.09] to 0.63 [0.59] ppb h^{-1} via the reaction of CH_3O_2 [methylperoxy radical] + NO in the daytime average HO_2 production rate, and 0.67 [0.61] to 4.32 [4.27] ppb h^{-1} via the reaction of HO_2 + NO

in the daytime average HO_2 loss rate in Beijing, Shanghai and Guangzhou. The above results suggest that the $P_{unknown}$ considerably enhanced the RO_x concentrations and accelerated RO_x cycles in the coastal regions of China, and could produce significant increases in concentrations of inorganic aerosols and secondary organic aerosols and further aggravate haze events in these regions.

1. Introduction

The hydroxyl radical (OH) is the dominant oxidant in the troposphere, initiating daytime photochemistry, removing the majority of reactive gases, and leading to the formation of secondary products [e.g. ozone (O_3), peroxyacyl nitrates (PANs) and aerosols] that can affect air quality, climate, and human health (Stone et al., 2012). OH is formed primarily through the photolysis of O_3, nitrous acid (HONO), hydrogen peroxide (H_2O_2), the reactions of O_3 with alkenes, and the HO_2 to OH conversion process (HO_2+NO) (Platt et al., 1980; Crutzen and Zimmermann, 1991; Atkinson and Aschmann, 1993; Fried et al., 1997; Paulson et al., 1997). Recent field experiments have found the contribution of the photolysis of HONO to daytime OH production can reach up to 56, 42, and 33% in urban, rural and forest areas, respectively (Ren et al., 2003; Kleffmann et al., 2005; Acker et al., 2006), more than that of the photolysis of O_3. However, most current air quality models fail to predict observed HONO concentrations, underestimating daytime HONO in particular (Czader et al., 2012; Gonçalves et al., 2012; Li et al., 2011), due to the incomplete knowledge of HONO sources.

It is generally accepted that the photolysis of HONO (Reaction R2) in the early morning could be a major source of OH. After sunrise, HONO mixing ratios are usually in low concentrations due to the strong photolysis of HONO. However, many field experiments have found daytime HONO mixing ratios that are unexpectedly higher than the theoretical steady value (~10 ppt), in both urban and rural areas: e.g. 0.15–1.50 ppb higher in Asia (Su et al., 2008; Wu et al.,2013; Spataro et al., 2013), 0.01–0.43 ppb higher in Europe (Kleffmann et al., 2005; Acker et al., 2007; Sörgel et al., 2011; Michoud et al., 2014), 0.02–0.81 ppb higher in North America (Zhou et al., 2002a,b; Ren et al., 2010; Villena et al., 2011; N. Zhang et al., 2012; Wong et al., 2012; VanderBoer et al., 2013), 2.00 ppb higher (maximum) in South America (Elshorbany et al., 2009), and 0.015–0.02 ppb higher in Antarctica (Kerbrat et al., 2012) (Fig. 1). These high HONO mixing ratios, particularly in the daytime, cannot be explained well by gas-phase production (Reaction R1), suggesting that an unknown daytime HONO source ($P_{unknown}$) could exist.

$$OH + NO \rightarrow HONO \quad (R1)$$

$$HONO + h\nu \rightarrow OH + NO \quad (R2)$$

$$HONO + OH \rightarrow NO_2 + H_2O \quad (R3)$$

The $P_{unknown}$ was calculated by Su et al. (2008) at Xinken (Guangzhou, China), with a maximum of 4.90 ppb h^{-1}. Spataro et al. (2013) proposed a $P_{unknown}$ value of 2.58 ppb h^{-1} in Beijing. In fact, $P_{unknown}$ values, ranging from 0.06 to 4.90 ppb h^{-1} have been obtained from many field studies across the globe, as shown in Fig. 1, suggesting $P_{unknown}$ could contribute greatly to the daytime production of OH and

hydroperoxyl radical (HO_2).

The most important formation pathway for nocturnal HONO could be the hydrolysis reaction of nitrogen dioxide (NO_2) on humid surfaces (Reaction R4) (Kleffmann et al., 1999; Alicke et al., 2002; Finlayson-Pitts et al., 2003):

$$2NO_2 + H_2O \rightarrow HONO + HNO_3 \quad (R4)$$

Ammann et al. (1998) found HONO formation via the heterogeneous reduction of NO_2 on the surface of soot (Reaction R5), and Reaction (R5) can be enhanced by irradiation (Monge et al., 2010):

$$NO_2 + red_{ads} \rightarrow HONO + ox_{ads} \quad (R5)$$

George et al. (2005) and Stemmler et al. (2006, 2007) showed the heterogeneous reduction of NO_2 on organic surfaces (Reaction R6) (e.g. humic acid) to produce HONO:

$$NO_2 + HC_{red} \rightarrow HONO + HC_{ox} \quad (R6)$$

Li et al. (2008) proposed a homogeneous reaction of photolytically excited NO_2 with H_2O (Reaction R7), but this reaction has been proven to be unimportant in the real atmosphere (Carr et al., 2009; Wong et al., 2011; Amedro et al., 2011). Zhang and Tao (2010) suggested the homogeneous nucleation of NO_2, H_2O and ammonia (NH_3) for the production of HONO (Reaction R8), but Reaction (R8) has not yet been tested in laboratory studies, nor observed in field experiments:

$$NO_2 + h\upsilon\ (\lambda > 420\ nm) \rightarrow NO_2^*$$

$$NO_2^* + H_2O \rightarrow HONO + OH \quad (R7)$$

$$NO_2^* + M \rightarrow NO_2 + M$$

$2NO_2 + H_2O(g) + NH_3 \rightarrow HONO + NH_4NO_3(s)$ (R8)

Zhou et al. (2002b, 2003, 2011) demonstrated that the photolysis of adsorbed nitric acid (HNO_3) and nitrate (NO_3^-) at ultraviolet wavelengths (~300 nm) (Reaction R9) can produce HONO:

$HNO_3/NO_3^- + h\upsilon \rightarrow HONO/ NO_2^- + O$ (R9)

Additionally, HONO could be emitted from soils (Su et al., 2011; Oswald et al., 2013), and may be important in farmland and forest areas.

Based on these mechanisms outlined above, some modeling studies have been carried out to simulate HONO concentrations (e.g. An et al., 2011; Czader et al., 2012; Gonçalves et al., 2012). Sarwar et al. (2008) incorporated Reactions (R4), (R9) and HONO emissions into the Community Multiscale Air Quality (CMAQ) model, but still underestimated HONO mixing ratios during daytime. Li et al. (2010) considered both aerosol and ground surface reactions, and HONO emissions in the WRF-Chem model (Weather Research and Forecasting model coupled with Chemistry), and found that HONO simulations were significantly improved. However, Li et al. (2010) used a relatively high emission ratio of 2.3% for $HONO/NO_2$ to compute the direct emissions of HONO, which could have overestimated the HONO concentrations in the air (An et al., 2013). Czader et al. (2012) added Reactions (R6), (R7) and HONO emissions into the CMAQ model. The HONO simulations matched well with observations at night, but were significantly lower than observations at noon. Wong et al. (2013) reported good agreement between simulated and observed daytime HONO when HONO emissions,

134 photolytically enhanced daytime formation mechanisms on both aerosols and the
135 ground, and Reaction R7 were included. However, according to our recent studies
136 (Tang et al., 2014), this result depended heavily on the selection of uptake
137 coefficients of NO_2 heterogeneous chemistry. Overall, the topic of HONO sources
138 remains under discussion today, and so it is a challenge for modelers to decide which
139 mechanism(s) to be coupled into an air quality model.

140 To investigate the importance of the mechanisms described above, correlation
141 tests between the $P_{unknown}$ and NO_2, HNO_3, irradiation or the photolysis frequency of
142 NO_2 [$J(NO_2)$] were conducted in field experiments (Acker et al., 2007; Sörgel et al.,
143 2011; Villena et al., 2011; Wong et al., 2012). Many of these studies demonstrated
144 that there is a clear dependency of the $P_{unknown}$ on irradiation/$J(NO_2)$ during daytime,
145 particularly at noon. Rohrer et al. (2005) proposed that the photolytic HONO source
146 at the surface of the chamber strongly depended on light intensity. Acker et al. (2007)
147 summarized field experiments in several European countries and showed a strong
148 correlation (R^2=0.81) between the $P_{unknown}$ and $J(NO_2)$. Wong et al. (2012) also
149 indicated that the $P_{unknown}$ showed a clear symmetrical diurnal variation with a
150 maximum around noontime, closely correlated with actinic flux (NO_2 photolysis
151 frequency) and solar irradiance; the correlation coefficient was over 0.70.

152 Besides irradiation/$J(NO_2)$, good correlations between the $P_{unknown}$ and NO_2
153 mixing ratios have been found from both field and laboratory studies, supporting the
154 viewpoint that NO_2 is the primary precursor of HONO. Through estimating the
155 $P_{unknown}$, Acker et al. (2007) speculated that the daytime HONO levels might be

explained by a fast electron transfer onto adsorbed NO_2. Sörgel et al. (2011) indicated that the conversion of NO_2 most likely accounted for light-induced HONO formation, about an order of magnitude stronger than HONO formation during nighttime. High correlations between the $P_{unknown}$ and NO_2 mixing ratios have also been found [e.g. R^2 = 0.77 in Qin et al. (2006), R^2 = 0.80 in Villena et al. (2011), and R^2 = 0.62 in Elshorbany et al. (2009)], indicating that the photosensitized conversion of NO_2 is more likely to be the daytime HONO source. This is the reason why the recent CalNex 2010 (California Research at the Nexus of Air Quality and Climate Change) study found a very strong positive correlation (R^2= 0.985) between HONO flux and the product of NO_2 concentration and solar radiation at the Bakersfield site (Ren et al., 2011).

Based on the studies introduced above, the $P_{unknown}$ calculated from field experiments may be a practical method to help quantify the daytime HONO source. In this study, field experiment data from 13 different field campaigns across the globe were used to express the $P_{unknown}$ as a function of NO_2 mixing ratios and $J(NO_2)$ (see Sect. 2.2). We then added the $P_{unknown}$ into the WRF-Chem model to assess the impacts of the $P_{unknown}$ on the concentrations and production and loss rates of HONO, OH, HO_2, and organic peroxy radicals (RO_2).

2. Data and methods

2.1 Observed data

Observed air temperature (TA), relative humidity (RH), wind speed (WS) and

direction (WD) near the ground were obtained from the National Climatic Data Center, China Meteorological Administration (H. Zhang et al., 2012). Surface mixing ratios of O_3 and NO_2 in Beijing were obtained from the Beijing Atmospheric Environmental Monitoring Action carried out by the Chinese Academy of Sciences (Li et al., 2011; Wang et al., 2014), except those in Guangzhou, which were sourced from Qin et al. (2009). HONO observations were conducted using two annular denuders at the campus of Peking University (PKU) (39°59′N, 116°18′E) in Beijing on 17–20 August 2007 (Spataro et al., 2013) and a long path absorption photometer at the Backgarden (BG) supersite (23°30′N, 113°10′E), about 60 km northwest of Guangzhou on 3–31 July 2006 (X. Li et al., 2012). The measurement systems are described in detail in Spataro et al. (2013) and X. Li et al. (2012). OH and HO_2 were measured by laser induced fluorescence at the BG supersite on 3–30 July 2006 (Lu et al., 2012).

2.2 Parameterization of HONO sources

Besides HONO gas-phase production from Reaction (R1), three additional HONO sources [HONO emissions, Reaction (R4) (nighttime), and the $P_{unknown}$] were coupled into the WRF-Chem model in this work.

HONO emissions were calculated using $[0.023 \times f_{DV} + 0.008 \times (1 - f_{DV})] \times f_{TS}$, where f_{DV} denotes the nitrogen oxides (NO_x) emission ratio of diesel vehicles to total vehicles, and f_{TS} is the NO_x emission ratio of the traffic source to all anthropogenic sources (Li et al., 2011; An et al., 2013; Tang et al., 2014). Reaction (R4) was inserted into the Carbon-Bond Mechanism Z (CBM-Z) during nighttime only. The

heterogeneous reaction rate was parameterized by $k = \left(\frac{a}{D_g} + \frac{4}{v\gamma} \right)^{-1} A_s$ (Jacob, 2000), where a is the radius of aerosols, v is the mean molecular speed of NO_2, D_g is a gas-phase molecular diffusion coefficient taken as 10^{-5} m^2 s^{-1}(Dentener and Crutzen, 1993), and A_s is the aerosol surface area per unit volume of air, calculated from aerosol mass concentrations and number density in each bin set by the Model for Simulating Aerosol Interactions and Chemistry (MOSAIC). Hygroscopic growth of aerosols was considered (Li et al., 2011).

Previous studies (Sörgel et al., 2011; Villena et al., 2011; Wong et al., 2012) have shown $P_{unknown} \propto [NO_2] \cdot J(NO_2)$. To quantify the relationship between the $P_{unknown}$ and NO_2 mixing ratios and irradiation, daytime $P_{unknown}$, NO_2 mixing ratios and $J(NO_2)$, based on all the available data sets from 13 different field campaigns across the globe (Table S1), were plotted in Fig. 2. As expected, good correlation (R^2 = 0.75) between the $P_{unknown}$ and NO_2 mixing ratios was obtained (Fig. 2a). Furthermore, the correlation between the $P_{unknown}$ and $NO_2 \cdot J(NO_2)$ was increased to 0.80, with a linear regression slope of 19.60 (Fig. 2b). For the coastal regions of China, the correlation between the $P_{unknown}$ and $NO_2 \cdot J(NO_2)$ was 0.48, with a linear regression slope of 17.37 (Fig. S2b in the Supplement), which is within the maximum $P_{unknown}$ uncertainty range of 25% (Table S1). The $P_{unknown}$ cloud be expressed as a function of NO_2 mixing ratios and $J(NO_2)$, i.e., $P_{unknown} \approx 19.60[NO_2] \cdot J(NO_2)$. This formula is very similar to $P_{unknown} \approx \alpha \cdot J(NO_2) \cdot [NO_2] \cdot [H_2O] \cdot (S/V_g + S/V_a)$ proposed by Su et al. (2008), and $P_{unknown} \approx 3.3 \times 10^{-8} [NO_2] \cdot Q_s$ suggested by Wong et al. (2012) as an additional

daytime source of HONO through analysis of observed data, where S/V_a is the aerosol surface area-to-volume ratio, S/V_g is the ground surface area-to-volume ratio, α is a fitting parameter, and Q_s is solar visible irradiance.

2.3 Model setup

Used in this study was the WRF-Chem model version 3.2.1 (Grell et al., 2005; Fast et al., 2006), with the CBM-Z (Zaveri and Peters, 1999) and the MOSAIC (Zaveri et al., 2008). The detailed physical and chemical schemes for the simulations can be found in Tang et al. (2014). Two domains with a horizontal resolution of 27 km were employed in this study: domain 1 covered East Asia, whereas domain 2 covered the coastal regions of China, including the Beijing–Tianjin–Hebei region (BTH), the Yangtze River delta (YRD), and the Pearl River delta (PRD) (Fig. 3). There were 28 vertical model layers from the ground to 50 hPa, and the first model layer was ~28 m above the ground. Meteorological initial and boundary conditions were obtained from the National Centers for Environmental Prediction (NCEP) 1 °×1 ° reanalysis dataset. Chemical initial and boundary conditions were constrained with the output of the Model for Ozone and Related chemical Tracers, version 4 (MOZART-4) (Emmons et al., 2010) every 6 h. Monthly anthropogenic emissions in 2006/2007 and biogenic emissions were the same as those used by Li et al. (2011) and An et al. (2013).

Six simulations (cases R, R_{wop}, and R_p performed for the entire months of August 2007 and July 2006) with a spin-up period of seven days were conducted in this study to assess the $P_{unknown}$ effects on the concentrations and budgets of HONO, OH, HO_2,

and RO_2. Case R only considered Reaction (R1) as a reference; Case R_{wop} included case R with HONO emissions, and Reaction (R4) only at night; case R_p contained case R_{wop} with the $P_{unknown}$ [$\approx 19.60[NO_2] \cdot J(NO_2)$]. The $P_{unknown}$ and Reaction (R4) were added to the CBM-Z, and diagnostic variables (i.e. production and loss rates of HONO, OH, HO_2, RO_2, O_3, and other species) were inserted into the CBM-Z to quantify the $P_{unknown}$ impacts on the budgets of HONO, OH, HO_2, and RO_2 (Wang et al., 2014).

3. Results and discussion

3.1 Comparison of simulations and observations

Simulations of TA, RH, WS and WD were compared with observations, as shown in Wang et al. (2014). The statistical metrics, i.e. mean bias (MB), mean error (ME), root-mean-square error (RMSE), normalized mean bias (NMB), normalized mean error (NME), index of agreement (IOA), and correlation coefficient (CC), were comparable with those of Wang et al. (2010) and L. Li et al. (2012) using the fifth-generation Pennsylvania State University/National Center for Atmospheric Research Mesoscale Model (MM5) and H. Zhang et al. (2012) using the WRF model. For O_3 in Beijing of the BTH region and Guangzhou of the PRD region, the NMB, NME and IOA were −22.80%, 58.70% and 0.79, respectively (Table 1 for case R), comparable to the values of 30.2% for NMB, 55.8% for NME and 0.91 for IOA reported in L. Li et al. (2012) using the CMAQ model. When HONO emissions, Reaction (R4) and the $P_{unknown}$ were included, the NMB, NME and IOA increased to −2.20%, 66.10% and 0.80, respectively (Table 1 for case R_p). The NO_2 fluctuations

were generally captured (Fig. 4) but the simulated amplitude of NO_2 was underestimated in some cases (Fig. 4). This underestimation could be related with the uncertainty of NO_x emissions. For case R, the NMB, NME and IOA for NO_2 were −13.50%, 42.10% and 0.57, respectively (Table 1), similar to the results of Wang et al. (2010) using the CMAQ model (NMB of −33.0%, NME of 50.0%, and IOA of 0.61). Compared with case R, NO_2 simulations were further underestimated for case R_p (Table 1 for case R_p) due to the underestimation of NO_x emissions in Guangzhou.

HONO simulations with the gas-phase production only (case R) were always substantially underestimated compared with observations (Fig. 5), similar to the results of Sarwar et al. (2008), Li et al. (2011) and An et al. (2013). When HONO emissions and Reaction (R4) were included, HONO simulations were significantly improved, especially at night (Fig. 5 and Table 2 for case R_{wop}). For Beijing, the nighttime RMSE and NME were reduced by 0.90×10^6 molecules cm^{-3} and 44.70%, whereas the NMB and IOA were increased by 50.00% and 0.29, respectively (Table 2). For Guangzhou, the nighttime RMSE and NME were reduced by 0.44×10^6 molecules cm^{-3} and 32.90%, and the NMB and IOA were enhanced by 58.80% and 0.18, respectively. When the $P_{unknown}$ was included, daytime HONO simulations were considerably improved (Fig. 5 and Table 2 for case R_p). Compared with case R_{wop}, the daytime NME in Beijing was reduced by 19.60%, and the NMB and IOA in Beijing were increased to −24.30% from −62.00% and 0.73 from 0.64, respectively (Table 2); the daytime NME in Guangzhou was reduced by 8.10%, and the NMB in

Guangzhou was increased to −61.20% from −76.50% (Table 2).

Simulated diurnal variations of OH and HO_2 showed consistent patterns with the observed data (Fig. 6). When HONO emissions and Reaction (R4) were considered (case R_{wop}), OH and HO_2 enhancements were minor in most cases compared with case R (Fig. 6 and Table 3), but the $P_{unknown}$ led to noticeable improvements in OH simulations on 5–12 July 2006 (Fig. 6). Substantial overestimation of OH mixing ratios on 20–25 July 2006 (Fig. 6) needs further investigation. Compared with case R, the NME was reduced by 79.60%, whereas the NMB was increased by 105.40%, and the IOA was improved to 0.84 from 0.79 (Table 3). When the $P_{unknown}$ was considered, HO_2 simulations were substantially improved (Fig. 6), the IOA was improved to 0.61 from 0.54 and the CC was improved to 0.66 from 0.57 (Table 3). However, HO_2 simulations were still substantially underestimated (Fig. 6). One of the major reasons for the HO_2 underestimation could be related to the considerable underestimation of anthropogenic volatile organic compounds (VOCs) (Wang et al., 2014).

3.2 $P_{unknown}$ simulations and its impacts on production and loss rates of HONO

High $P_{unknown}$ values were found in the coastal regions of China (Fig. 7), especially in the BTH, YRD and PRD regions due to elevated emissions of NO_x (Zhang et al., 2009). For the BTH region, the largest daytime average $P_{unknown}$ values reached 2.5 ppb h^{-1} in Tianjin (Fig. 7a). Elevated daytime average $P_{unknown}$ values were found in the YRD region, with a maximum of 2.0 ppb h^{-1} in Shanghai (Fig. 7b). Daytime average $P_{unknown}$ values reached 1.2 ppb h^{-1} in Guangzhou and Shenzhen of

the PRD (Fig. 7c). The simulated $P_{unknown}$ values in the PRD region were lower than those in the BTH and YRD regions. One major reason is the underestimation of daytime NO_2 mixing ratios in the PRD (Fig. 4b).

For case R, daytime HONO production was primarily from the reaction of OH and NO (Reaction R1), with a maximum production rate of 0.69 ppb h^{-1} in Beijing, 1.20 ppb h^{-1} in Shanghai, and 0.72 ppb h^{-1} in Guangzhou near noon due to high OH mixing ratios (Fig. 8a, c, e). The loss rate of HONO was 0.62 ppb h^{-1} in Beijing, 1.09 ppb h^{-1} in Shanghai, and 0.65 ppb h^{-1} in Guangzhou via Reaction (R2), much higher than the 0.01–0.02 ppb h^{-1} in Beijing, Shanghai and Guangzhou via Reaction (R3) (Fig. 8b, d, f), indicating that Reaction (R2) accounted for approximately 99% of the total loss rate of HONO.

When the additional HONO sources [HONO emissions, Reaction (R4), and the $P_{unknown}$] were coupled into the WRF-Chem model, nighttime HONO was formed mainly via Reaction (R4) (0.30–1.42 ppb h^{-1} in Beijing, 0.20–0.45 ppb h^{-1} in Shanghai, and 0.25–0.84 ppb h^{-1} in Guangzhou) (Fig. 8a, c, e). HONO emissions contributed 0.04–0.62 ppb h^{-1} to HONO production (Fig. 8a, c, e). Simulated $P_{unknown}$ values ranged from 0.42 to 2.98 ppb h^{-1} in Beijing, from 0.18 to 2.58 ppb h^{-1} in Shanghai, and from 0.06 to 1.66 ppb h^{-1} in Guangzhou (Fig. 8a, c, e). The simulated $P_{unknown}$ values in Beijing (Fig. 8a) were in good agreement with the results of Spataro et al. (2013), with an average unknown daytime HONO production rate of 2.58 ppb h^{-1} in the studied summer period. However, the simulated $P_{unknown}$ values in Guangzhou (Fig. 8e) were lower than the 2.36–4.90 ppb h^{-1} reported by Su

et al (2008), due mainly to the underestimation of the daytime NO_2 mixing ratios in the PRD region. The additional HONO sources produce more HONO, which subsequently photolyzes to yield more OH. Therefore, the formation of HONO through Reaction (R1) was greatly enhanced, with a maximum of 4.70 [1.44 due to the $P_{unknown}$] ppb h^{-1} in Beijing, 4.25 [3.13] ppb h^{-1} in Shanghai, and 1.58 [0.40] ppb h^{-1} in Guangzhou in the morning (Fig. 8a, c, e), much higher than the 0.69 ppb h^{-1} in Beijing, 1.20 ppb h^{-1} in Shanghai, and 0.72 ppb h^{-1} in Guangzhou, respectively, for case R (Fig. 8a, c, e). Meanwhile, the loss rate of HONO via Reaction (R2) was significantly enhanced, with a maximum enhancement of 5.20 (= 5.82 − 0.62) [1.97 due to the $P_{unknown}$] ppb h^{-1} in Beijing, 4.31 (= 5.40 − 1.09) [1.44] ppb h^{-1} in Shanghai, and 1.96 (= 2.61 − 0.65) [1.18] ppb h^{-1} in Guangzhou (Fig. 8b, d, f). The HONO loss rate via dry deposition ranged from 0.28 to 0.45 ppb h^{-1} (not shown), roughly equivalent to the contribution of HONO emissions, suggesting that dry deposition of HONO cannot be neglected in high NO_x emission areas. The maximum $P_{unknown}$ uncertainty range of 25% (Table S1), a 25% increase (decrease) in the slope factor (19.60) led to a 9.19−18.62% increase (12.69−14.32% decrease) in the maximum HONO production rate and a 0−17.64% increase (8.40−14.07% decrease) in the maximum HONO loss rate (Fig. S3 in the Supplement).

3.3 $P_{unknown}$ impacts on concentrations of OH, HO_2 and RO_2

Incorporation of the $P_{unknown}$ into the WRF-Chem model led to substantial enhancements in the daytime average mixing ratios of OH in the coastal regions of China, e.g. 60–190% in the BTH region, 60–210% in the YRD region, and 60–200%

in the PRD region (Fig. 9a). The maximum enhancement of HO_2 reached 250% in the BTH region, 200% in the YRD region, and 140% in the PRD region (Fig. 9b). Similarly, a maximum increase of 180, 150 and 80% in RO_2 [= CH_3O_2 (methylperoxy radical) + ETHP (ethylperoxy radical) + C_2O_3 (peroxyacyl radical) + others] were found in the BTH, YRD and PRD regions, respectively (Fig. 9c).

Vertically, the $P_{unknown}$ enhanced the monthly meridional-mean daytime (06:00–18:00 LST) mixing ratios of OH, HO_2 and RO_2 by 5–38, 5–47 and 5–48%, respectively, within 1000 m above the ground in the coastal regions of China (Fig. 10). The vertical enhancements of OH, HO_2 and RO_2 at the same latitude were roughly uniform within the 1000 m (Fig. 10) due to strong vertical mixing in the daytime. Different $P_{unknown}$ distributions led to distinct differences in the enhancements of OH, HO_2 and RO_2, with a maximum located near 35 °N (Fig. 10).

3.4 $P_{unknown}$ impacts on the budgets of OH, HO_2 and RO_2

OH radicals are produced mainly through the reaction of HO_2 + NO, the photolysis of O_3 and HONO, and the reactions between O_3 and alkenes (Fig. 11). For case R, the predominant contribution to P(OH) [production rate of OH] was the reaction of HO_2 + NO, with a diurnal peak of 4.04 ppb h^{-1} in Beijing, 1.52 ppb h^{-1} in Shanghai, and 3.91 ppb h^{-1} in Guangzhou at noon (Fig. S1a, c, e in the Supplement). The photolysis of O_3 was the second most important sources of OH, which was dominant (0.91 ppb h^{-1} in Beijing, 0.52 ppb h^{-1} in Shanghai, and 1.20 ppb h^{-1} in Guangzhou) at noon (Fig. S1a, c, e). Compared with the two OH sources above, the contributions of the reactions of O_3 + alkenes, HONO photolysis and others were

small, lower than 0.15 ppb h^{-1} (Fig. S1a, c, e). When the additional HONO sources were added, the most important source was the reaction of HO_2 + NO, with a diurnal maximum conversion rate reaching 9.38 [7.23 due to the $P_{unknown}$] ppb h^{-1} in Beijing, 2.63 [1.15] ppb h^{-1} in Shanghai, and 4.88 [1.43] ppb h^{-1} in Guangzhou near noon (Fig. 11a, c, e). The photolysis of HONO became the second important source of OH in Beijing and Guangzhou before 10:00 LST, and in Shanghai before 12:00 LST; the diurnal peaks were 3.72 [3.06] ppb h^{-1} in Beijing at 09:00 LST, 0.89 [0.62] ppb h^{-1} in Shanghai at 11:00 LST, and 0.97 [0.78] ppb h^{-1} in Guangzhou at 09:00 LST (Fig. 11a, c, e), which were comparable to or lower than the 3.10 ppb h^{-1} reported by Elshorbany et al. (2009). The contributions of the photolysis of O_3, the reactions of O_3 + alkenes and others to P(OH) showed minor changes in comparison with case R (Figs. 11a, c, e and S1a, c, e). Kanaya et al. (2009), who also conducted similar studies at Mount Tai (located in a rural area) of China, suggested that the reaction of HO_2 + NO was the predominant OH source, with a daytime average of 3.72 ppb h^{-1}, more than the 1.38 ppb h^{-1} of the photolysis of O_3. Hens et al. (2014) reported similar results in a boreal forest, in which the dominant contributor to OH was the reaction of HO_2 + NO, ranging from 0.23 to 1.02 ppb h^{-1} during daytime. The production rates of OH in our study were higher than in Kanaya et al. (2009) and Hens et al. (2014) due to higher NO_x emissions in urban areas than in rural areas.

The dominant loss rate of OH was the reaction of OH + NO_2 for both cases R and R_p (Figs. 11b, d, f and S1b, d, f). The diurnal maximum loss rates were 1.98 ppb h^{-1} in Beijing, 1.12 ppb h^{-1} in Shanghai, and 1.70 ppb h^{-1} in Guangzhou for case R

(Fig. S1b, d, f), whereas these values were 5.61 [4.38 due to the $P_{unknown}$] ppb h^{-1} in Beijing, 2.00 [1.00] ppb h^{-1} in Shanghai, and 2.65 [1.02] ppb h^{-1} in Guangzhou for case R_p (Fig. 11b, d, f). The reactions of OH + VOCs to form HO_2 and RO_2 were the second most important loss path of OH, with a diurnal maximum of 0.75–1.73 ppb h^{-1} for case R (Fig. S1b, d, f) and 1.57 [0.82 due to the $P_{unknown}$] to 5.37 [4.05] ppb h^{-1} for case R_p in Beijing, Shanghai and Guangzhou (Fig. 11b, d, f). The third most important OH loss path was the reaction of OH + CO to form HO_2; the diurnal maximum rates were 0.46–1.47 ppb h^{-1} for case R (Fig. S1b, d, f) and 0.93 [0.49 due to the $P_{unknown}$] to 3.58 [2.86] ppb h^{-1} for case R_p in Beijing, Shanghai and Guangzhou (Fig. 11b, d, f).

The averaged radical conversion rates in the daytime (06:00–18:00 LST) are illustrated in Fig. 12. OH radicals are produced mainly via the photolysis of O_3, HONO and hydrogen peroxide (H_2O_2), and the reactions between O_3 and alkenes, after which OH radicals enter the RO_x (= OH + HO_2 + RO_2) cycle (Fig. 12 and Tables 4, S2 and S3 in the Supplement). In the cycle, the transfer among OH, HO_2 and RO_2 radicals oxidizes VOCs and converts NO to NO_2, accomplishing major oxidation processes. The OH, HO_2 and RO_2 radicals are eliminated by the termination reactions, ultimately leading to the formation and deposition of reservoir species (e.g. HNO_3, organic acid, PANs, and H_2O_2).

For case R, the reaction of HO_2 + NO was the major source of OH [2.78 ppb h^{-1} (81.73% of the total daytime average production rate of OH) in Beijing, 0.73 ppb h^{-1} (67.09%) in Shanghai, and 1.75 ppb h^{-1} (71.54%) in Guangzhou] (Fig. 12a and Table

4). The second largest source of OH was the photolysis of O_3 [0.47 ppb h^{-1} (13.68%) in Beijing, 0.31 ppb h^{-1} (28.17%) in Shanghai, and 0.62 ppb h^{-1} (25.27%) in Guangzhou] (Table 4). OH radicals were removed mainly through the reaction of OH + NO_2 [1.12 ppb h^{-1} (39.31% of the total daytime average loss rate of OH) in Beijing, 0.47 ppb h^{-1} (46.63%) in Shanghai, and 0.77 ppb h^{-1} (38.33%) in Guangzhou] (Table 4), whereas those were converted to HO_2 mainly via the reaction of OH + CO [0.79 ppb h^{-1} (27.65%) in Beijing, 0.20 ppb h^{-1} (19.97%) in Shanghai, and 0.58 ppb h^{-1} (28.67%) in Guangzhou] (Table 4). The total daytime average conversion rate of OH to HO_2 was 0.40–1.35 ppb h^{-1}, and that of OH to RO_2 was 0.21–0.69 ppb h^{-1} in Beijing, Shanghai and Guangzhou (Fig. 12a). For HO_2, the predominant production pathways were the reactions of OH + CO [0.79 ppb h^{-1} (33.42%) in Beijing, 0.20 ppb h^{-1} (28.27%) in Shanghai, and 0.58 ppb h^{-1} (38.26%) in Guangzhou] and CH_3O_2 + NO [0.54 ppb h^{-1} (23.12%) in Beijing, 0.16 ppb h^{-1} (22.53%) in Shanghai, and 0.33 ppb h^{-1} (21.75%) in Guangzhou] and the photolysis of formaldehyde (HCHO) [0.24 ppb h^{-1} (10.34%) in Beijing, 0.09 ppb h^{-1} (11.97%) in Shanghai, and 0.11 ppb h^{-1} (7.42%) in Guangzhou] (Table S2). HO_2 radicals were consumed primarily via the reaction of HO_2 + NO [2.78 ppb h^{-1} (99.34%) in Beijing, 0.73 ppb h^{-1} (99.61%) in Shanghai, and 1.75 ppb h^{-1} (98.29%) in Guangzhou] (Table S2). RO_2 radicals were formed mainly from the reactions of OH + OLET (terminal olefin carbons)/OLEI (internal olefin carbons) [0.19 ppb h^{-1} (22.45%) in Beijing, 0.05 ppb h^{-1} (21.07%) in Shanghai, and 0.06 ppb h^{-1} (14.88%) in Guangzhou], OH + ETH (ethene) [0.16 ppb h^{-1} (18.36%) in Beijing, 0.03 ppb h^{-1} (11.91%) in Shanghai,

and 0.04 ppb h^{-1} (10.24%) in Guangzhou], OH + methane (CH_4) [0.10 ppb h^{-1} (12.09%) in Beijing, 0.06 ppb h^{-1} (22.44%) in Shanghai, and 0.14 ppb h^{-1} (33.97%) in Guangzhou], and OH + AONE (acetone) [0.09 ppb h^{-1} (10.76%) in Beijing, 0.02 ppb h^{-1} (7.09%) in Shanghai, and 0.05 ppb h^{-1} (11.24%) in Guangzhou]. RO_2 radicals were consumed primarily via the reaction of CH_3O_2 + NO [0.54 ppb h^{-1} (94.56%) in Beijing, 0.16 ppb h^{-1} (95.28%) in Shanghai, and 0.33 ppb h^{-1} (96.07%) in Guangzhou] (Table S3).

When the additional HONO sources were inserted into the WRF-Chem model (case R_p), the daytime average OH production rate was enhanced by 4.32 (= 7.10 − 2.78) [3.86 due to the $P_{unknown}$] ppb h^{-1} in Beijing, 0.67 (= 1.40 − 0.73) [0.64] ppb h^{-1} in Shanghai, and 0.80 (= 2.55 − 1.75) [0.68] ppb h^{-1} in Guangzhou via the reaction of HO_2 + NO, and by 1.86 (= 1.86 − 0) [1.86] ppb h^{-1} in Beijing, 0.50 (= 0.50 − 0) [0.50] ppb h^{-1} in Shanghai, and 0.49 (= 0.49 − 0) [0.47] ppb h^{-1} in Guangzhou via the photolysis of HONO, respectively (Table 4). The enhancements of the daytime average OH production rate due to the photolysis of HONO were comparable to or lower than the 2.20 ppb h^{-1} obtained by Liu et al. (2012). The daytime average OH loss rate was increased by 2.03 (= 3.15 − 1.12) [1.92 due to the $P_{unknown}$] ppb h^{-1} in Beijing, 0.58 (= 1.05 − 0.47) [0.55] ppb h^{-1} in Shanghai, and 0.65 (= 1.42 − 0.77) [0.58] ppb h^{-1} in Guangzhou via the reaction of OH + NO_2, and by 1.78 (= 2.57 − 0.79) [1.64] ppb h^{-1} in Beijing, 0.31 (= 0.51 − 0.20) [0.28] ppb h^{-1} in Shanghai, and 0.42 (= 1.00 − 0.58) [0.36] ppb h^{-1} in Guangzhou via the reaction of OH + CO, respectively (Table 4). Similarly, the daytime average HO_2 production rate was

increased by 0.31 [0.28 due to the $P_{unknown}$] to 1.78 [1.64] ppb h^{-1} in Beijing, Shanghai and Guangzhou via the reaction of OH + CO, and by 0.63 (= 1.17 − 0.54) [0.59] ppb h^{-1} in Beijing, 0.10 (= 0.26 − 0.16) [0.09] ppb h^{-1} in Shanghai, and 0.19 (= 0.52 − 0.33) [0.17] ppb h^{-1} in Guangzhou via the reaction of CH_3O_2 + NO; whereas, the daytime average HO_2 loss rate was enhanced by 0.67 [0.61 due to the $P_{unknown}$] to 4.32 [4.27] ppb h^{-1} in Beijing, Shanghai and Guangzhou via the reaction of HO_2 + NO (Table S2). The additional HONO sources also led to an increase of 0.06 (= 0.11 − 0.05) [0.04 due to the $P_{unknown}$] to 0.35 (= 0.54 − 0.19) [0.28] ppb h^{-1} via the reaction of OH + OLET/OLEI, 0.04 (= 0.07 − 0.03) [0.03] to 0.32 (= 0.48 − 0.16) [0.28] ppb h^{-1} via the reaction of OH + ETH, 0.06 (= 0.12 − 0.06) [0.06] to 0.16 (= 0.26 − 0.10) [0.15] ppb h^{-1} via the reaction of OH + CH_4, and 0.03 (= 0.05 − 0.02) [0.03] to 0.23 (= 0.32 − 0.09) [0.21] ppb h^{-1} via the reaction of OH + AONE in the daytime average RO_2 production rate, and 0.10 [0.09 due to the $P_{unknown}$] to 0.63 [0.59] ppb h^{-1} via the reaction of CH_3O_2 + NO in the daytime average RO_2 loss rate in Beijing, Shanghai and Guangzhou (Table S3).

Overall, the net daytime production rate of RO_x was increased to 3.48 (= 2.56 + 0.71 + 0.21) [2.06 due to the $P_{unknown}$] from 1.20 (= 0.60 + 0.43 + 0.17) ppb h^{-1} in Beijing, 1.09 (= 0.86 + 0.19 + 0.04) [0.45] from 0.54 (= 0.36 + 0.14 + 0.04) ppb h^{-1} in Shanghai, and 1.52 (= 1.21 + 0.26 + 0.05) [0.58] from 0.92 (= 0.68 + 0.20 + 0.04) ppb h^{-1} in Guangzhou (Fig. 12) due to the additional HONO sources, indicating that the RO_x source was mainly from OH production, especially via the photolysis of HONO (Tables 4, S2 and S3). This result is different from the conclusion of Liu et al.

(2012) that the photolysis of HONO and oxygenated VOCs is the largest RO_x source. One of the primary reasons for this is the underestimation of anthropogenic VOCs (Wang et al., 2014). For Beijing, the net production rate of RO_x was 3.48 ppb h^{-1}, lower than the 6.60 ppb h^{-1} from the field studies of Liu et al. (2012). Our results reconfirmed the view of Ma et al. (2012) that the North China Plain acts as an oxidation pool. The additional HONO sources produced an increase in the net loss rate of RO_x from 1.25 (= 1.23 + 0.01 + 0.01) to 3.28 (3.24+0.03+0.01) [1.96 due to the $P_{unknown}$] ppb h^{-1} in Beijing, 0.53 (= 0.51 + 0.01 + 0.01) to 1.09 (= 1.07 + 0.01 + 0.01) [0.54] ppb h^{-1} in Shanghai, and 0.85 (= 0.82 + 0.02 + 0.01) to 1.51 (= 1.47 + 0.03 + 0.01) [0.59] ppb h^{-1} in Guangzhou (Fig. 12).

4. Conclusions

The relationship between the $P_{unknown}$, NO_2 mixing ratios and $J(NO_2)$ was investigated using available data from 13 field studies across the globe. The formula $P_{unknown} \approx 19.60[NO_2] \cdot J(NO_2)$ was obtained, and then the additional HONO sources (i.e., the $P_{unknown}$, HONO emissions and nighttime hydrolysis conversion of NO_2 on aerosols) were inserted into the WRF-Chem model, to assess the $P_{unknown}$ impacts on the concentrations and budgets of HONO and RO_x in the coastal regions of China. The results showed that:

(1) The additional HONO sources led to significant improvements in the simulations of HONO and OH, especially in the daytime.

(2) Elevated daytime average $P_{unknown}$ values were found in the coastal regions of China, reaching 2.5 ppb h^{-1} in the BTH region, 2.0 ppb h^{-1} in the YRD region,

and 1.2 ppb h^{-1} in the PRD region.

(3) When the additional HONO sources were considered, nighttime HONO was produced primarily via Reaction (R4) (0.20–1.42 ppb h^{-1} in Beijing, Shanghai and Guangzhou). Simulated $P_{unknown}$ values lay between 0.42 and 2.98 ppb h^{-1} in Beijing, between 0.18 and 2.58 ppb h^{-1} in Shanghai, and between 0.06 and 1.66 ppb h^{-1} in Guangzhou. HONO emissions contributed 0.04–0.62 ppb h^{-1} to HONO production.

(4) The additional HONO sources substantially enhanced the production and loss rates of HONO. The maximum production rate of HONO was increased to 4.70 [1.44 due to the $P_{unknown}$] from 0.69 ppb h^{-1} in Beijing, 4.25 [3.13] from 1.20 ppb h^{-1} in Shanghai, and 1.58 [0.40] from 0.72 ppb h^{-1} in Guangzhou via the reaction of OH and NO in the morning; whereas, the maximum loss rate of HONO was increased to 5.82 [1.97] from 0.62 ppb h^{-1} in Beijing, 5.40 [1.44] from 1.09 ppb h^{-1} in Shanghai, and 2.61 [1.18] from 0.65 ppb h^{-1} in Guangzhou via the photolysis of HONO. Dry deposition of HONO contributed 0.28–0.45 ppb h^{-1} to the loss rate of HONO, approximately equivalent to the contribution of HONO emissions, emphasizing the importance of dry deposition of HONO in high NO_x emission areas.

(5) The $P_{unknown}$ produced a 60–210% enhancement of OH, a 60–250% enhancement of HO_2, and a 60–180% enhancement of RO_2 near the ground in the major cities of the coastal regions of China. Vertically, the $P_{unknown}$ enhanced the daytime meridional-mean mixing ratios of OH, HO_2 and RO_2 by 5–38, 5–47 and 5–48%, respectively, within 1000 m above the ground.

(6) When the additional HONO sources were added, the photolysis of HONO

became the second important source of OH in Beijing and Guangzhou before 10:00 LST, and in Shanghai before 12:00 LST, with a maximum of 3.72 [3.06 due to the $P_{unknown}$] ppb h^{-1} in Beijing, 0.89 [0.62] ppb h^{-1} in Shanghai, and 0.97 [0.78] ppb h^{-1} in Guangzhou; whereas, the reaction of HO_2 + NO was the most important source of OH, dominated in Beijing and Guangzhou after 10:00 LST and in Shanghai after 12:00 LST, with a maximum of 9.38 [7.23] ppb h^{-1} in Beijing, 2.63 [1.15] ppb h^{-1} in Shanghai, and 4.88 [1.43] ppb h^{-1} in Guangzhou.

(7) The additional HONO sources, especially the $P_{unknown}$, accelerated the whole RO_x cycle. The daytime average OH production rates were enhanced by 4.32 [3.86 due to the $P_{unknown}$] ppb h^{-1} in Beijing, 0.67 [0.64] ppb h^{-1} in Shanghai, and 0.80 [0.68] ppb h^{-1} in Guangzhou via the reaction of HO_2 + NO, and by 1.86 [1.86] ppb h^{-1} in Beijing, 0.50 [0.50] ppb h^{-1} in Shanghai, and 0.49 [0.47] ppb h^{-1} in Guangzhou via the photolysis of HONO. The daytime average OH loss rates were increased by 2.03 [1.92 due to the $P_{unknown}$] ppb h^{-1} in Beijing, 0.58 [0.55] ppb h^{-1} in Shanghai, and 0.65 [0.58] ppb h^{-1} in Guangzhou via the reaction of OH + NO_2, and by 1.78 [1.64] ppb h^{-1} in Beijing, 0.31 [0.28] ppb h^{-1} in Shanghai, and 0.42 [0.36] ppb h^{-1} in Guangzhou via the reaction of OH + CO.

(8) The additional HONO sources produced an increase of 0.31 [0.28 due to the $P_{unknown}$] to 1.78 [1.64] ppb h^{-1} via the reaction of OH + CO and 0.10 [0.09] to 0.63 [0.59] ppb h^{-1} via the reaction of CH_3O_2 + NO in the daytime average HO_2 production rate, and 0.67 [0.61] to 4.32 [4.27] ppb h^{-1} via the reaction of HO_2 + NO in the daytime average HO_2 loss rate in Beijing, Shanghai and Guangzhou. Similarly,

552 the additional HONO sources led to an enhancement of 0.06 [0.04] to 0.35 [0.28]
553 ppb h^{-1} via the reaction of OH + OLET/OLEI, 0.04 [0.03] to 0.32 [0.28] ppb h^{-1} via
554 the reaction of OH + ETH, 0.06 [0.06] to 0.16 [0.15] ppb h^{-1} via the reaction of OH
555 + CH_4, and 0.03 [0.03] to 0.23 [0.21] ppb h^{-1} via the reaction of OH + AONE in the
556 daytime average RO_2 production rate, and 0.10 [0.09] to 0.63 [0.59] ppb h^{-1} via the
557 reaction of CH_3O_2 + NO in the daytime average RO_2 loss rate in Beijing, Shanghai
558 and Guangzhou.

559 Overall, the above results suggest that the $P_{unknown}$ significantly enhances the
560 atmospheric oxidation capacity in the coastal regions of China by increasing RO_x
561 concentrations and accelerating RO_x cycles, and could lead to considerable increases
562 in concentrations of inorganic aerosols and secondary organic aerosols and further
563 aggravate haze events in these regions.

564

565 **Acknowledgements**

566 This research was partially supported by the National Natural Science Foundation of
567 China (41175105, 41405121), a Key Project of the Chinese Academy of Sciences
568 (XDB05030301), and the Carbon and Nitrogen Cycle Project of the Institute of
569 Atmospheric Physics, Chinese Academy of Sciences, and the Beijing Municipal
570 Natural Science Foundation (8144054).

571

572

573

References

Acker, K., Möller, D.: Corrigendum to: Atmospheric variation of nitrous acid at different sites in Europe. Environmental Chemistry, 4(5), 364-364, 2007.

Acker, K., Möller, D., Wieprecht, W., Meixner, F. X., Bohn, B., Gilge, S., Plass-Dülmer, C., and Berresheim, H.: Strong daytime production of OH from HNO_2 at a rural mountain site, Geophys. Res. Lett., 33(2), doi: 10.1029/2005GL024643, 2006.

Alicke, B., Platt, U., and Stutz, J.: Impact of nitrous acid photolysis on the total hydroxyl radical budget during the limitation of oxidant production/Pianura padana produzione di ozono study in Milan, J. Geophys. Res. –Atmos., 107(D22): LOP9-1 – LOP9-17, doi: 10.1029/2000JD000075, 2002.

Amedro, D., Parker, A. E., Schoemaecker, C., Fittschen, C.: Direct observation of OH radicals after 565nm multi-photon excitation of NO_2 in the presence of H_2O. Chemical Physics Letters, 513(1), 12-16, 2011.

Ammann, M., Kalberer, M., Jost, D. T., Tobler, L., Rössler, E., Piguet, D., Gäggeler, H., Baltensperger, U.: Heterogeneous production of nitrous acid on soot in polluted air masses. Nature, 395(6698), 157-160, 1998.

An, J., Li, Y., Wang, F., and Xie, P.: Impacts of photoexcited NO_2 chemistry and heterogeneous reactions on concentrations of O_3 and NO_y in Beijing, Tianjin and Hebei province of China, Air Quality-Models and Applications, Prof. Dragana Popovic (Ed.), InTech, ISBN: 978-953-307-307-1, doi: 10.5772/16858, 2011.

An, J., Li, Y., Chen, Y., Li, J., Qu, Y., Tang, Y.: Enhancements of major aerosol components due to additional HONO sources in the North China Plain and implications for visibility and haze. Advances in Atmospheric Science, 30, 57-66, 2013.

Atkinson, R., Aschmann, S. M.: Hydroxyl radical production from the gas-phase reactions of ozone with a series of alkenes under atmospheric conditions. Environmental science & technology, 27(7), 1357-1363, 1993.

Carr, S., Heard, D., Blitz, M.: Comment on "Atmospheric Hydroxyl Radical Production from Electronically Excited NO_2 and H_2O". Science, 324, 5925, doi:10.1126/science.1166669, 2009.

Crutzen, P. J., Zimmermann, P. H.: The changing photochemistry of the troposphere. Tellus B, 43(4), 136-151, 1991.

Czader, B. H., Rappenglück, B., Percell, P., Byun, D. W., Ngan, F., Kim, S.: Modeling nitrous acid and its impact on ozone and hydroxyl radical during the Texas Air Quality Study 2006. Atmospheric Chemistry and Physics, 12(15), 6939-6951, 2012.

Dentener, F. J., Crutzen, P. J.: Reaction of N_2O_5 on tropospheric aerosols: Impact on the global distributions of NO_x, O_3, and OH. Journal of Geophysical Research: Atmospheres (1984–2012), 98(D4), 7149-7163, 1993.

Elshorbany, Y. F., Kurtenbach, R., Wiesen, P., Lissi, E., Rubio, M., Villena, G., Gramsch, E., Rickard, A. R., Pilling, M. J., Kleffmann, J.: Oxidation capacity of the city air of Santiago, Chile. Atmospheric Chemistry and Physics, 9(6),

618 2257-2273, 2009.
619 Emmons, L. K., Walters, S., Hess, P. G., Lamarque, J. F., Pfister, G. G., Fillmore, D.,
620 Granier, C., Guenther, A., Kinnison, D., Laepple, T., Orlando, J., Tie, X.,
621 Tyndall, G., Wiedinmyer, C., Baughcum, S. L., Kloster, S.: Description and
622 evaluation of the Model for Ozone and Related chemical Tracers, version 4
623 (MOZART-4). Geoscientific Model Development, 3(1), 43-67, 2010.
624 Fast, J. D., Gustafson, W. I., Easter, R. C., Zaveri, R. A., Barnard, J. C., Chapman, E.
625 G., Grell, G. A., and Peckham, S. E.: Evolution of ozone, particulates, and
626 aerosol direct radiative forcing in the vicinity of Houston using a fully coupled
627 meteorology chemistry aerosol model, J. Geophys. Res. –Atmos., 111(D21), doi:
628 10.1029/2005JD006721, 2006.
629 Finlayson-Pitts, B. J., Wingen, L. M., Sumner, A. L., Syomin, D., Ramazan, K. A.:
630 The heterogeneous hydrolysis of NO_2 in laboratory systems and in outdoor and
631 indoor atmospheres: An integrated mechanism.Physical Chemistry Chemical
632 Physics, 5(2), 223-242, 2003.
633 Fried, A., McKeen, S., Sewell, S., Harder, J., Henry, B., Goldan, P., Kuster, W.,
634 William, E., Baumann, K., Shett, R., Cantrell, C.: Photochemistry of
635 formaldehyde during the 1993 Tropospheric OH Photochemistry
636 Experiment. Journal of Geophysical Research: Atmospheres
637 (1984–2012), 102(D5), 6283-6296, 1997.
638 George, C., Strekowski, R. S., Kleffmann, J., Stemmler, K., Ammann, M.:
639 Photoenhanced uptake of gaseous NO_2 on solid organic compounds: a

photochemical source of HONO?. Faraday discussions, 130, 195-210, 2005.

Gonçalves, M., Dabdub, D., Chang, W. L., Jorba, O., Baldasano, J. M.: Impact of HONO sources on the performance of mesoscale air quality models. Atmospheric Environment, 54, 168-176, 2012.

Grell, G. A., Peckham, S. E., Schmitz, R., McKeen, S. A., Frost, G., Skamarock, W. C., Eder, B.: Fully coupled "online" chemistry within the WRF model. Atmospheric Environment, 39(37), 6957-6975, 2005.

Hens, K., Novelli, A., Martinez, M., Auld, J., Axinte, R., Bohn, B., Fischer, H., Keronen, P., Kubistin, D., Nölscher, A. C., Oswald, R., Paasonen, P., Petäjä, T., Regelin, E., Sander, R., Sinha, V., Sipilä, M., Taraborrelli, D., Tatum Ernest, C., Williams, J., Lelieveld, J., Harder, H.: Observation and modeling of HO_x radicals in a boreal forest. Atmospheric Chemistry and Physics, 14, 8723–8747, 2014.

Jacob, D. J.: Heterogeneous chemistry and tropospheric ozone. Atmospheric Environment, 34(12), 2131-2159, 2000.

Kanaya, Y., Pochanart, P., Liu, Y., Li, J., Tanimoto, H., Kato, S., Suthawaree. J., Inomata, S., Taketani, F., Okuzawa, K., Kawamura, K., Akimoto, H., Wang, Z. F.: Rates and regimes of photochemical ozone production over Central East China in June 2006: a box model analysis using comprehensive measurements of ozone precursors. Atmospheric Chemistry and Physics, 9, 7711–7723, 2009.

Kerbrat, M., Legrand, M., Preunkert, S., Galléé, H., and Kleffmann, J.: Nitrous acid at Concordia (inland site) and Dumont d'Urville (coastal site), East Antarctica,

662 J. Geophys. Res. –Atmos., 117(D8), doi: 10.1029/2011JD017149, 2012.
663 Kleffmann, J., Gavriloaiei, T., Hofzumahaus, A., Holland, F., Koppmann, R., Rupp,
664 L.,Schlosser, E., Siese, M., and Wahner, A.: Daytime formation of nitrous acid:
665 a major source of OH radicals in a forest, J. Geophys. Res. Lett., 32(5), doi:
666 10.1029/2005GL022524, 2005.
667 Kleffmann, J., Gavriloaiei, T., Hofzumahaus, A., Holland, F., Koppmann, R., Rupp,
668 L., Schlosser, E., Siese, M., Wahner, A.: Daytime formation of nitrous acid: A
669 major source of OH radicals in a forest. Geophysical Research Letters, 32(5),
670 2005.
671 Li, G., Lei, W., Zavala, M., Volkamer, R., Dusanter, S., Stevens, P., Molina1, L. T.:
672 Impacts of HONO sources on the photochemistry in Mexico City during the
673 MCMA-2006/MILAGO Campaign. Atmospheric Chemistry and Physics, 10,
674 6551–6567, 2010.
675 Li, L., Chen, C. H., Huang, C., Huang, H. Y., Zhang, G. F., Wang, Y. J., Wang,
676 H. L., Lou, S. R., Qiao, L. P., Zhou, M., Chen, M. H., Chen, Y. R., Fu,
677 J. S., Streets, D. G., Jang, C. J.: Process analysis of regional ozone formation
678 over the Yangtze River Delta, China using the Community Multi-scale Air
679 Quality modeling system. Atmospheric Chemistry and Physics, 12,
680 10971-10987, 2012.
681 Li, S., J. Matthews, and A. Sinha.: Atmospheric hydroxyl radical production from
682 electronically excited NO_2 and H_2O. Science, 319, 1657–1660, 2008.
683 Li, X., Brauers, T., Häseler, R., Bohn, B., Fuchs, H., Hofzumahaus, A., Holland, F.,

Lou, S., Lu, K. D., Rohrer, F., Hu, M., Zeng, L. M., Zhang, Y. H., Garland, R. M., Su, H., Nowak, A., Wiedensohler, A., Takegawa, N., Shao, M., Wahner, A.: Exploring the atmospheric chemistry of nitrous acid (HONO) at a rural site in Southern China. Atmospheric Chemistry and Physics, 12(3), 1497-1513, 2012.

Li, Y., An, J., Min, M., Zhang, W., Wang, F., Xie, P.: Impacts of HONO sources on the air quality in Beijing, Tianjin and Hebei Province of China. Atmospheric Environment, 45(27), 4735-4744, 2011.

Liu, Z., Wang, Y., Gu, D., Zhao, C., Huey, L. G., Sticke, R., Liao, J., Shao, M., Zhu, T., Zeng, L., Amoroso, A., Costabile, F., Chang, C.-C., Liu, S.-C.: Summertime photochemistry during CARE Beijing-2007: RO_x budgets and O_3 formation. Atmospheric Chemistry and Physics, 12, 7737–7752, 2012.

Lu, K. D., Rohrer, F., Holland, F., Fuchs, H., Bohn, B., Brauers, T., Chang, C. C., Haseler, R., Hu, M., Kita, K., Kondo, Y., Li, X., Lou, S. R., Nehr, S., Shao, M., Zeng, L. M., Wahner, A., Zhang, Y. H., Hofzumahaus, A.: Observation and modelling of OH and HO_2 concentrations in the Pearl River Delta 2006: a missing OH source in a VOC rich atmosphere. Atmospheric Chemistry and Physics, 12(3), 1541-1569, 2012.

Ma, J. Z., Wang, W., Chen, Y., Liu, H. J., Yan, P., Ding, G. A., Wang, M. L., Sun, J., Lelieveld, J.: The IPAC-NC field campaign: a pollution and oxidization pool in the lower atmosphere over Huabei, China. Atmospheric Chemistry and Physics, 12, 3883–3908, 2012.

Michoud, V., Colomb, A., Borbon, A., Miet, K., Beekmann, M., Camredon, M.,

706 Aumont, B., Perrier, S., Zapf, P., Siour, G., Ait-Helal, W., Afif, C., Kukui, A.,
707 Furger, M., Dupont, J. C., Haeffelin, M., Doussin, J. F.: Study of the unknown
708 HONO daytime source at a European suburban site during the MEGAPOLI
709 summer and winter field campaigns. Atmospheric Chemistry and Physics, 14(6),
710 2805-2822, 2014.
711 Monge, M. E., D'Anna, B., Mazri, L., Giroir-Fendler, A., Ammann, M., Donaldson,
712 D. J., George, C.: Light changes the atmospheric reactivity of soot. Proceedings
713 of the National Academy of Sciences, 107(15), 6605-6609, 2010.
714 Oswald, R., Behrendt, T., Ermel, M., Wu, D., Su, H., Cheng, Y., Breuninger, C.,
715 Moravek, A., Mougin, E., Delon, C., Loubet, B., Pommerening-Röser, A.,
716 Sörgel, M., Pöschl, U., Hoffmann, T., Andreae, M.O., Meixner, F.X., Trebs, I.:
717 HONO emissions from soil bacteria as a major source of atmospheric reactive
718 nitrogen. Science 341, 1233-1235, 2013.
719 Paulson, S. E., Sen, A. D., Liu, P., Fenske, J. D., Fox, M. J.: Evidence for formation
720 of OH radicals from the reaction of O_3 with alkenes in the gas
721 phase. Geophysical research letters, 24(24), 3193-3196, 1997.
722 Platt, U., Perner, D., Harris, G. W., Winer, A. M., Pitts, J. N.: Observations of
723 nitrous acid in an urban atmosphere by differential optical absorption.
724 Nature 285, 312-314 (29 May 1980); doi: 10.1038/285312a0, 1980.
725 Qin, M., Xie, P. H., Liu, W. Q., Li, A., Dou, K., Fang, W., Liu, J., Zhang, W. J.:
726 Observation of atmospheric nitrous acid with DOAS in Beijing, China. Journal
727 of Environmental Sciences, 18(1), 69-75, 2006.

728 Qin, M., Xie, P., Su, H., Gu, J., Peng, F., Li, S., Zengb, L., Liua, J., Liua W., Zhang,
729 Y.: An observational study of the HONO–NO_2 coupling at an urban site in
730 Guangzhou City, South China. Atmospheric Environment, 43(36), 5731-5742,
731 2009.
732 Ren, X., Gao, H., Zhou, X., Crounse, J. D., Wennberg, P. O., Browne, E. C.,
733 LaFranchi, B. W., Cohen, R. C., McKay, M., Goldstein, A. H., Mao, J.:
734 Measurement of atmospheric nitrous acid at Bodgett Forest during
735 BEARPEX2007. Atmospheric Chemistry and Physics, 10(13), 6283-6294,
736 2010.
737 Ren, X., Harder, H., Martinez, M., Lesher, R. L., Oliger, A., Simpas, J. B., Brunea,
738 W. H., Schwab, J. J., Demerjian, K. L., He, Y., Zhou, X., Gao, H.: OH and HO_2
739 Chemistry in the urban atmosphere of New York City. Atmospheric
740 Environment, 37(26), 3639-3651, 2003.
741 Ren, X., Sanders, J. E., Rajendran, A., Weber, R. J., Goldstein, A.H., Pusede, S. E.,
742 Browne, E. C., Min, K.-E., and Cohen, R.C.: A relaxed eddy accumulation
743 system for measuring vertical fluxes of nitrous acid, Atmos. Meas. Tech., 4,
744 2093–2103, doi:10.5194/amt-4-2093-2011, 2011.
745 Rohrer, F., Bohn, B., Brauers, T., Brüning, D., Johnen, F. J., Wahner, A., Kleffmann,
746 J.: Characterisation of the photolytic HONO-source in the atmosphere
747 simulation chamber SAPHIR. Atmospheric Chemistry and Physics, 5(8),
748 2189-2201, 2005.
749 Sörgel, M., Regelin, E., Bozem, H., Diesch, J. M., Drewnick, F., Fischer, H., Harder,

H., Held, A., Hosaynali-Beygi, Z., Martinez, M., Zetzsch, C.: Quantification of the unknown HONO daytime source and its relation to NO_2. Atmospheric Chemistry and Physics, 11(20), 10433-10447, 2011.

Sarwar, G., Roselle, S. J., Mathur, R., Appel, W., Dennis, R. L., Vogel, B.: A comparison of CMAQ HONO predictions with observations from the Northeast Oxidant and Particle Study. Atmospheric Environment, 42(23), 5760-5770, 2008.

Spataro, F., Ianniello, A., Esposito, G., Allegrini, I., Zhu, T., Hu, M.: Occurrence of atmospheric nitrous acid in the urban area of Beijing (China).Science of the Total Environment, 447, 210-224, 2013.

Stemmler, K., Ammann, M., Donders, C., Kleffmann, J., George, C.: Photosensitized reduction of nitrogen dioxide on humic acid as a source of nitrous acid. Nature, 440(7081), 195-198, 2006.

Stemmler, K., Ndour, M., Elshorbany, Y., Kleffmann, J., D'anna, B., George, C., Bohn, B., Ammann, M.: Light induced conversion of nitrogen dioxide into nitrous acid on submicron humic acid aerosol. Atmospheric Chemistry and Physics, 7(16), 4237-4248, 2007.

Stone, D., Whalley, L. K., Heard, D. E.: Tropospheric OH and HO_2 radicals: field measurements and model comparisons. Chemical Society Reviews, 41, 6348-6404, 2012.

770 Su, H., Cheng, Y., Oswald, R., Behrendt, T., Trebs, I., Meixner, F. X., Andreae, M.
771 O., Cheng, P., Zhang, Y., Pöschl, U.: Soil nitrite as a source of atmospheric
772 HONO and OH radicals. Science, 333(6049), 1616-1618, 2011.
773 Su, H., Cheng, Y. F., Shao, M., Gao, D. F., Yu, Z. Y., Zeng, L. M., Slanina, J., Zhang,
774 Y. H., and Wiedensohler, A.: Nitrous acid (HONO) and its daytime sources at a
775 rural site during the 2004 PRIDE-PRD experiment in China, J. Geophys. Res.
776 –Atmos., 113(D14), doi: 10.1029/2007JD009060, 2008.
777 Tang, Y., An, J., Li, Y., Wang, F.: Uncertainty in the uptake coefficient for HONO
778 formation on soot and its impacts on concentrations of major chemical
779 components in the Beijing–Tianjin–Hebei region. Atmospheric Environment,
780 84, 163-171, 2014.
781 VandenBoer, T. C., Brown, S. S., Murphy, J. G., Keene, W. C., Young, C. J.,
782 Pszenny, A. A. P., Kim, S., Warneke, C., de Gouw, J. A., Maben, J. R., Wagner,
783 N. L., Riedel, T. P., Thornton, J. A., Wolfe, D. E., Dubé, W. P., Öztürk, F.,
784 Brock, C. A., Grossberg, N., Lefer, B., Lerner, B. Middlebrook, A. M., Roberts,
785 J. M.: Understanding the role of the ground surface in HONO vertical structure:
786 High resolution vertical profiles during NACHTT-11. Journal of Geophysical
787 Research: Atmospheres, 118, 10,155–10,171, doi:10.1002/jgrd.50721, 2013.
788 Villena, G., Wiesen, P., Cantrell, C. A., Flocke, F., Fried, A., Hall, S. R., Hornbrook,
789 R. S., Knapp, D., Kosciuch, E., Mauldin, R. L., McGrath, J. A., Montzka, D.,
790 Richter, D., Ullmann, K., Walega, J., Weibring, P., Weinheimer, A., Staebler, R.
791 M., Liao, J., Huey, L. G., and Kleffmann, J.: Nitrous acid (HONO) during polar

792 spring in Barrow, Alaska: a net source of OH radicals?, J. Geophys. Res.
793 –Atmos., 116(D14), doi: 10.1029/2011JD016643, 2011.
794 Wang, F., An, J., Li, Y., Tang, Y., Lin, J., Qu, Y., Cheng, Y., Zhang, B., Zhai, J.:
795 Impacts of Uncertainty in AVOC Emissions on the Summer RO_x Budget and
796 Ozone Production Rate in the Three Most Rapidly-Developing Economic
797 Growth Regions of China. Advances in Atmospheric Sciences, 31, 1331–1342,
798 2014.
799 Wang, X., Zhang, Y., Hu, Y., Zhou, W., Lu, K., Zhong, L., Zeng, L., Shao, M., Hu,
800 M., Russell, A. G.: Process analysis and sensitivity study of regional ozone
801 formation over the Pearl River Delta, China, during the PRIDE-PRD2004
802 campaign using the Community Multiscale Air Quality modeling
803 system. Atmospheric Chemistry and Physics, 10(9), 4423-4437, 2010.
804 Wong, K. W., Oh, H. J., Lefer, B. L., Rappenglück, B., Stutz, J.: Vertical profiles of
805 nitrous acid in the nocturnal urban atmosphere of Houston, TX. Atmospheric
806 Chemistry and Physics, 11(8), 3595-3609, 2011.
807 Wong, K. W., Tsai, C., Lefer, B., Grossberg, N., Stutz, J.: Modeling of daytime
808 HONO vertical gradients during SHARP 2009. Atmospheric Chemistry and
809 Physics, 13(7), 3587-3601, 2013.
810 Wong, K. W., Tsai, C., Lefer, B., Haman, C., Grossberg, N., Brune, W. H., Ren,
811 X., Luke, W., Stutz, J.: Daytime HONO vertical gradients during SHARP 2009
812 in Houston, TX. Atmospheric Chemistry and Physics, 12(2), 635-652, 2012.
813 Wu, J., Xu, Z., Xue, L., Wang, T.: Daytime nitrous acid at a polluted suburban site

814 in Hong Kong: Indication of heterogeneous production on aerosol. Proceedings
815 of 12th international conference on atmospheric sciences and applications to air
816 quality, Seoul, Korea, June 3-5, 2013, p. 52, 2013.
817 Zaveri, R. A., Peters, L. K.: A new lumped structure photochemical mechanism for
818 large‐scale applications. Journal of Geophysical Research: Atmospheres
819 (1984–2012), 104(D23), 30387-30415, 1999.
820 Zaveri, R. A., Easter, R. C., Fast, J. D., and Peters, L. K.: Model for simulating
821 aerosol interactions and chemistry (MOSAIC), J. Geophys. Res. –Atmos.,
822 113(D13), doi: 10.1029/2007JD008782, 2008.
823 Zhang, B., Tao, F.: Direct homogeneous nucleation of NO_2, H_2O, and NH_3 for the
824 production of ammonium nitrate particles and HONO gas. Chemical Physics
825 Letters, 489, 4-6, 143, 2010.
826 Zhang, H., Li, J., Ying, Q., Yu, J. Z., Wu, D., Cheng, Y., Kebin Hed, Jiang, J.:
827 Source apportionment of $PM_{2.5}$ nitrate and sulfate in China using a
828 source-oriented chemical transport model. Atmospheric Environment, 62,
829 228-242, 2012.
830 Zhang, N., Zhou, X., Bertman, S., Tang, D., Alaghmand, M., Shepson, P. B., Carroll,
831 M. A.: Measurements of ambient HONO concentrations and vertical HONO
832 flux above a northern Michigan forest canopy. Atmospheric Chemistry and
833 Physics, 12(17), 8285-8296, 2012.
834 Zhang, Q., Streets, D. G., Carmichael, G. R., He, K., Huo, H., Kannari, A., Klimont,
835 Z., Park, I., Reddy, S., Fu, J. S., Chen, D., Duan, L., Lei, Y., Wang, L., Yao, Z.:

836 Asian emissions in 2006 for the NASA INTEX-B mission. Atmospheric
837 Chemistry and Physics, 9, 5131-5153, 2009.
838 Zhou, X., Civerolo, K., Dai, H., Huang, G., Schwab, J., and Demerjian, K:
839 Summertime nitrous acid chemistry in the atmospheric boundary layer at a rural
840 site in New York State, J. Geophys. Res. –Atmos., 107(D21), ACH13-1 –
841 ACH13-11, doi: 10.1029/2001JD001539, 2002a.
842 Zhou, X., Gao, H., He, Y., Huang, G., Bertman, S. B., Civerolo, K., and Schwab, J.:
843 Nitric acid photolysis on surfaces in low-NO_x environments: significant
844 atmospheric implications, Geophys. Res. Lett., 30(23), doi:
845 10.1029/2003GL018620, 2003.
846 Zhou, X., He, Y., Huang, G., Thornberry, T. D., Carroll, M. A., and Bertman, S. B.:
847 Photochemical production of nitrous acid on glass sample manifold surface,
848 Geophys. Res. Lett., 29, 26-1 – 26-4, doi: 10.1029/2002GL015080, 2002b.
849 Zhou, X., Zhang, N., TerAvest, M., Tang, D., Hou, J., Bertman, S., Alaghmand, M.,
850 Shepson, P. B. Carroll, M. A. Griffith, S., Dusanter, S., Stevens, P. S.: Nitric
851 acid photolysis on forest canopy surface as a source for tropospheric nitrous
852 acid. Nature Geoscience, 4(7), 440-443, 2011.

Table 1. Model performance statistics for O_3 and NO_2 in Beijing in August 2007 and Guangzhou in July 2006.

Species	Case	MB (ppb)	ME (ppb)	RMSE (ppb)	NMB (%)	NME (%)	IOA
O_3	R_p	−0.65	19.40	25.44	−2.20	66.10	0.80
	R	−6.69	17.21	25.24	−22.80	58.70	0.79
NO_2	R_p	−9.50	17.31	21.40	−29.10	53.00	0.51
	R	−4.40	13.75	17.61	−13.50	42.10	0.57

MB: mean bias; ME: mean error; RMSE: root-mean-square error; NMB: normalized mean bias; NME: normalized mean error; IOA: index of agreement.

Table 2. Model performance statistics for daytime (06:00–18:00 LST) and nighttime (19:00–05:00 LST) HONO in Beijing in August 2007 and Guangzhou in July 2006.

Species	Case	MB (10^6 molec cm^{-3})	ME (10^6 molec cm^{-3})	RMSE (10^6 molec cm^{-3})	NMB (%)	NME (%)	IOA	CC
$HONO_{daytime}$ (Beijing)	R_p	−0.54	0.98	1.41	−24.30	44.50	0.73	0.57
	R_{wop}	−1.37	1.41	1.83	−62.00	64.10	0.64	0.63
	R	−2.07	2.07	2.58	−93.80	93.80	0.46	0.31
$HONO_{nighttime}$ (Beijing)	R_p	−0.73	0.84	1.09	−42.20	49.10	0.77	0.74
	R_{wop}	−0.82	0.91	1.16	−47.90	53.20	0.75	0.75
	R	−1.68	1.68	2.06	−97.90	97.90	0.46	0.76
$HONO_{daytime}$ (Guangzhou)	R_p	−0.38	0.43	0.58	−61.20	69.60	0.58	0.56
	R_{wop}	−0.48	0.49	0.65	−76.50	77.70	0.55	0.56
	R	−0.60	0.60	0.80	−95.60	96.20	0.43	-0.30
$HONO_{nighttime}$ (Guangzhou)	R_p	−0.42	0.75	1.05	−32.90	58.50	0.66	0.43
	R_{wop}	−0.49	0.83	1.15	−38.40	64.30	0.63	0.38
	R	−1.25	1.25	1.59	−97.20	97.20	0.45	-0.01

CC: correlation coefficient.

867 Table 3. Model performance statistics for OH and HO_2 in Guangzhou in July 2006.

Species	Case	MB (10^6 molec cm^{-3})	ME (10^6 molec cm^{-3})	RMSE (10^6 molec cm^{-3})	NMB (%)	NME (%)	IOA	CC
OH	R_p	−1.35	4.37	6.22	−17.60	57.00	0.84	0.75
	R_{wop}	−3.00	4.58	6.25	−112.20	126.50	0.81	0.72
	R	−3.36	4.85	6.55	−123.00	136.60	0.79	0.70
HO_2	R_p	−3.80	3.81	5.59	−78.50	78.60	0.61	0.66
	R_{wop}	−4.19	4.20	6.14	−86.60	86.70	0.54	0.59
	R	−4.22	4.23	6.16	−87.20	87.30	0.54	0.57

868

869

870

871

872

873

874

875 Table 4. Daytime (06:00–18:00 LST) average OH budgets in Beijing/Shanghai/Guangzhou in August 2007.
876

Reaction	Case R		Case R_{wop}		Case R_p	
	Rate (ppb h^{-1})	Contribution (%)	Rate (ppb h^{-1})	Contribution (%)	Rate (ppb h^{-1})	Contribution (%)
OH production						
HO_2+NO	**2.778/0.732/1.748**	**81.73/67.09/71.54**	**3.242/0.760/1.871**	**83.74/68.00/72.02**	**7.101/1.402/2.553**	**73.34/61.95/67.55**
***$(HONO+hv)_{net}$**	**--/--/--**	**--/--/--**	**--/--/0.017**	**--/--/0.66**	**1.855/0.497/0.489**	**19.16/21.98/12.93**
O^1D+H_2O	**0.465/0.307/0.617**	**13.68/28.17/25.27**	**0.479/0.306/0.630**	**12.36/27.38/24.24**	**0.568/0.312/0.651**	**5.86/13.80/17.23**
O_3+OLET/OLEI	0.101/0.024/0.027	2.98/2.16/1.11	0.095/0.023/0.027	2.45/2.08/1.03	0.080/0.021/0.025	0.83/0.91/0. 65
*$(H_2O_2+hv)_{net}$	0.035/0.023/0.029	1.02/2.07/1.17	0.035/0.023/0.030	0.91/2.03/1.16	0.037/0.022/0.032	0.38/0.97/0.19
HO_2+O_3	0.009/0.001/0.014	0.28/0.07/0.59	0.010/0.001/0.015	0.26/0.06/0.58	0.026/0.001/0.019	0.27/0.05/0.51
*$(HNO_3+hv)_{net}$	0.005/0.001/0.002	0.15/0.06/0.10	0.005/0.001/0.002	0.13/0.06/0.09	0.007/0.001/0.003	0.07/0.04/0.07
ROOH+hv	0.003/0.004/0.005	0.09/0.36/0.19	0.003/0.004/0.005	0.09/0.38/0.19	0.007/0.007/0.007	0.07/0.29/0.19
O_3+ETH	0.002/<0.001/<0.001	0.05/0.02/0.01	0.002/<0.001/<0.001	0.04/0.02/0.01	0.001/<0.001/<0.001	0.02/0.01/0.01
HO_2+NO_3	<0.001/<0.001/<0.001	<0.01/<0.01/0.01	<0.001/<0.001/<0.001	<0.01/<0.01/<0.01	<0.001/<0.001/<0.001	<0.01/<0.01/<0.01
O_3+ISOP	<0.001/<0.001/<0.001	0.01/<0.01/<0.01	<0.001/<0.001/<0.001	0.01/<0.01/<0.01	<0.001/<0.001/<0.001	<0.01/<0.01/<0.01
Total	3.399/1.091/2.443	100/100/100	3.873/1.118/2.598	100/100/100	9.683/2.263/3.779	100/100/100
OH loss						
OH+NO_2	**1.116/0.474/0.770**	**39.31/46.63/38.33**	**1.225/0.501/0.844**	**38.11/45.86/38.86**	**3.146/1.045/1.424**	**38.08/44.29/40.76**
OH+CO	**0.785/0.203/0.576**	**27.65/19.97/28.67**	**0.932/0.227/0.637**	**29.00/20.78/29.33**	**2.573/0.506/1.001**	**31.14/21.45/28.65**
OH+OLET/OLEI	**0.192/0.054/0.059**	**6.76/5.31/2.94**	**0.264/0.065/0.077**	**8.21/5.95/3.55**	**0.537/0.206/0.095**	**6.50/8.73/2.72**
OH+HCHO	**0.150/0.050/0.146**	**5.28/4.92/7.27**	**0.166/0.053/0.156**	**5.16/4.85/7.18**	**0.544/0.096/0.242**	**6.59/4.07/6.93**
OH+CH_4	0.103/0.057/0.135	3.63/5.61/6.72	0.109/0.059/0.142	3.39/5.40/6.54	0.260/0.115/0.223	3.15/4.87/6.38
OH+ALD2/MGLY/ANOE	0.092/0.018/0.045	3.24/1.77/2.24	0.109/0.020/0.049	3.39/1.83/2.26	0.323/0.047/0.081	3.91/1.99/2.32
OH+SO_2	0.054/0.030/0.035	1.90/2.95/1.74	0.064/0.034/0.041	1.99/3.11/1.89	0.172/0.116/0.072	2.08/4.92/2.06

OH+XYL	0.052/0.022/0.023	1.83/2.16/1.14	0.066/0.026/0.029	2.05/2.38/1.34	0.141/0.078/0.045	1.71/3.31/1.29
OH+H_2	0.038/0.021/0.050	1.34/2.07/2.49	0.040/0.022/0.052	1.24/2.01/2.39	0.095/0.027/0.075	1.15/1.14/2.15
OH+TOL	0.027/0.007/0.011	0.95/0.69/0.55	0.034/0.008/0.014	1.06/0.73/0.64	0.086/0.025/0.024	1.04/1.06/0.69
OH+HONO	0.003/0.003/0.005	0.11/0.30/0.25	0.006/0.004/0.007	0.19/0.37/0.32	0.069/0.023/0.032	0.84/0.97/0.92
OH+HNO_x	0.005/0.001/0.005	0.18/0.10/0.25	0.005/0.001/0.005	0.16/0.09/0.23	0.015/0.002/0.008	0.18/0.08/0.23
OH+O_3	0.028/0.006/0.035	0.99/0.59/1.70	0.029/0.006/0.036	0.90/0.55/1.66	0.072/0.005/0.046	0.87/0.21/1.32
OH+H_2O_2	0.015/0.008/0.027	0.53/0.79/1.34	0.016/0.008/0.029	0.50/0.73/1.34	0.040/0.010/0.043	0.48/0.42/1.23
OH+ETH/OPEN	0.007/0.002/0.004	0.25/0.20/0.20	0.008/0.002/0.005	0.25/0.18/0.23	0.036/0.009/0.011	0.44/0.38/0.31
OH+CH_3OOH/ROOH	0.010/0.011/0.014	0.35/1.08/0.70	0.011/0.012/0.014	0.34/1.10/0.64	0.022/0.020/0.022	0.27/0.85/0.63
OH+ISOP	0.019/0.004/0.002	0.67/0.39/0.10	0.020/0.004/0.003	0.62/0.37/0.14	0.017/0.007/0.003	0.21/0.30/0.09
OH+PAR	0.005/0.002/0.004	0.18/0.20/0.20	0.007/0.003/0.005	0.22/0.27/0.23	0.015/0.005/0.007	0.18/0.21/0.20
OH+ONIT /ISOPRD	0.028/0.005/0.016	0.99/0.49/0.80	0.030/0.005/0.018	0.93/0.46/0.83	0.077/0.013/0.025	0.93/0.55/0.72
OH+C_2H_6	0.002/0.001/0.002	0.07/0.10/0.10	0.003/0.001/0.002	0.09/0.09/0.09	0.008/0.002/0.004	0.10/0.08/0.11
OH+CH_3OH/ANOL/CRES	0.002/0.001/0.002	0.07/0.10/0.10	0.002/0.001/0.002	0.06/0.09/0.09	0.007/0.002/0.003	0.08/0.08/0.09
OH+HO_2	0.001/<0.001/0.004	0.04/0.05/0.20	0.002/<0.001/0.005	0.06/0.05/0.23	0.006/<0.001/0.008	0.07/0.02/0.23
OH+NO	0.105/0.036/0.039	3.70/3.54/1.94	0.066/0.030/--	2.05/2.75/--	--/--/--	--/--/--
Total	2.839/1.017/2.009	100/100/100	3.214/1.093/2.172	100/100/100	8.261/2.360/3.495	100/100/100

OLET: internal olefin carbons (C=C); OLEI: terminal olefin carbons (C=C); ROOH: higher organic peroxide; ETH: ethene; ISOP: isoprene; ALD2: acetaldehyde; MGLY: methylglyoxal; ANOE: acetone; XYL: xylene; TOL: toluene; HNO_x: HNO_3 + HNO_4; OPEN: aromatic fragments; PAR: paraffin carbon –C–; ONIT: organic nitrate; ISOPRD: lumped intermediate species; ANOL: ethanol; CRES: cresol and higher molar weight phenols.

*The reactions of HONO+hv, H_2O_2+hv and HNO_3+hv are reversible, “net” in the subscript means subtracting the corresponding reverse reactions.

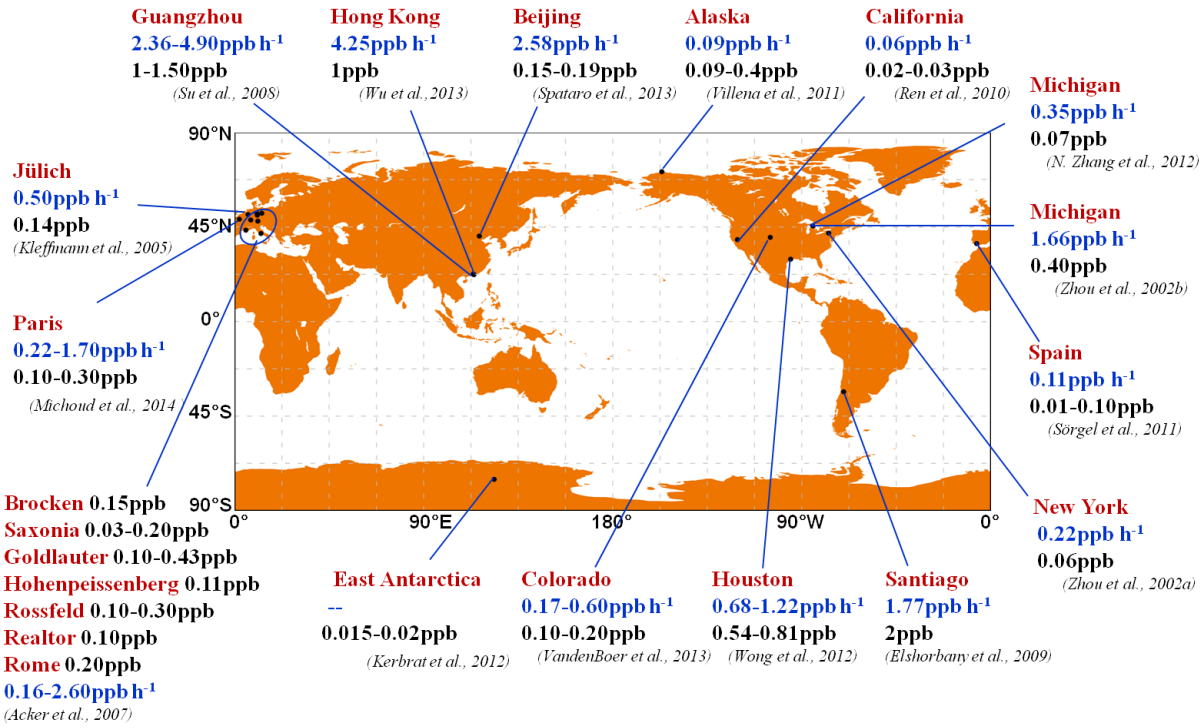

Fig. 1. Summary of observed HONO mixing ratios at noon (black font) and the calculated unknown daytime HONO source (blue font) from field studies.

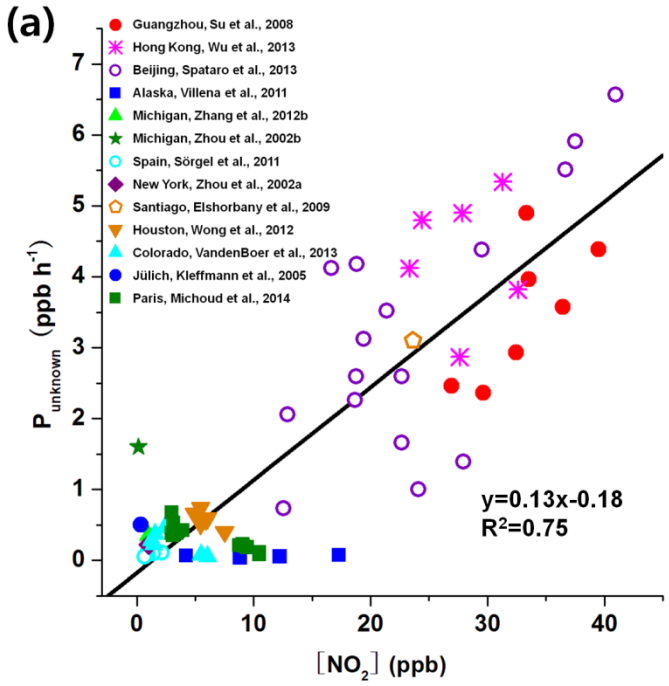

898

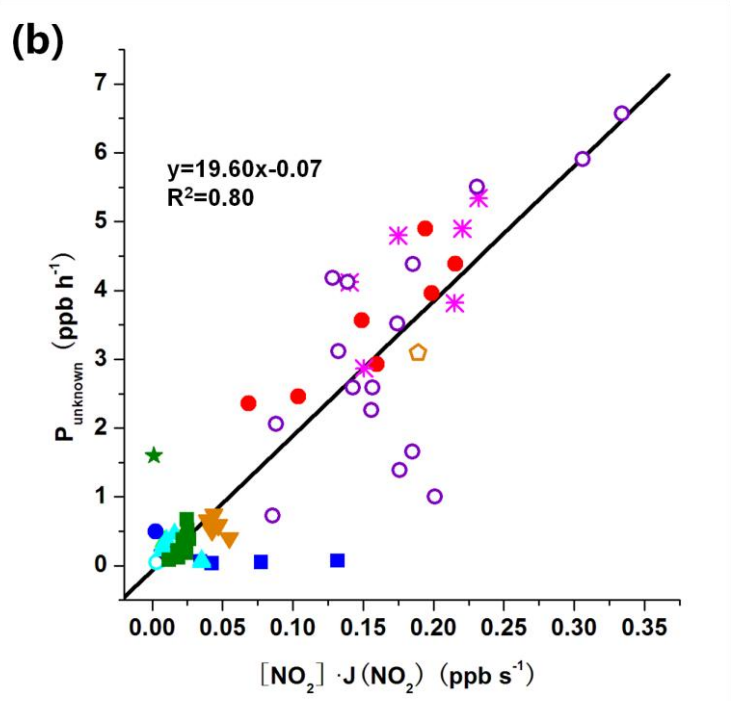

899

900 Fig. 2. Correlation of the unknown daytime HONO source ($P_{unknown}$) (ppb h^{-1}) with (a)

901 NO_2 (ppb) and (b) $NO_2 \times J(NO_2)$ (ppb s^{-1}), based on the field experiment data shown

902 in Fig. 1.

903

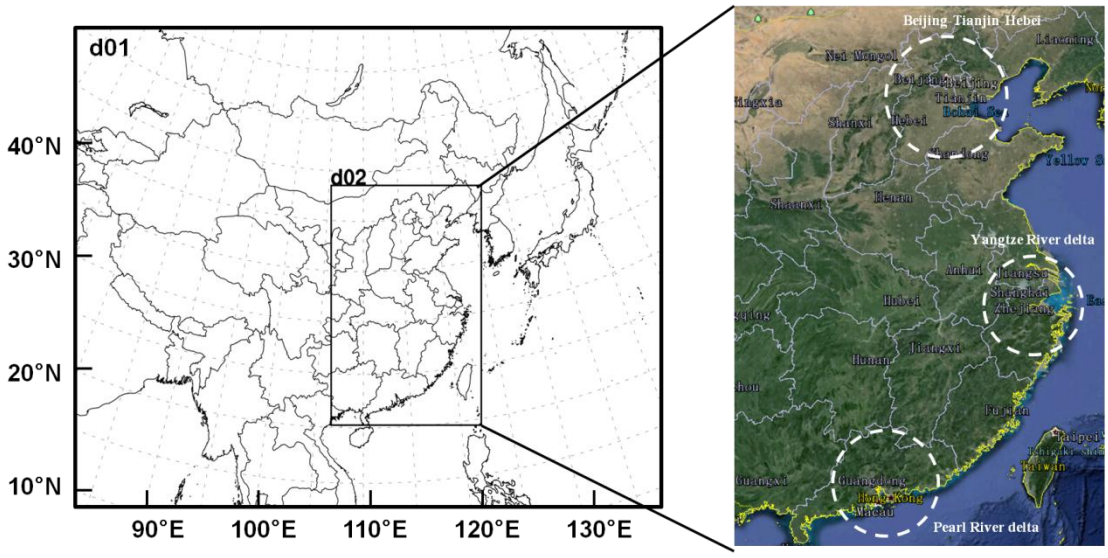

Fig. 3. Model domains used in this study. Domain 2 covers the Beijing–Tianjin–Hebei (BTH), Yangtze River delta (YRD), and Pearl River delta (PRD) regions.

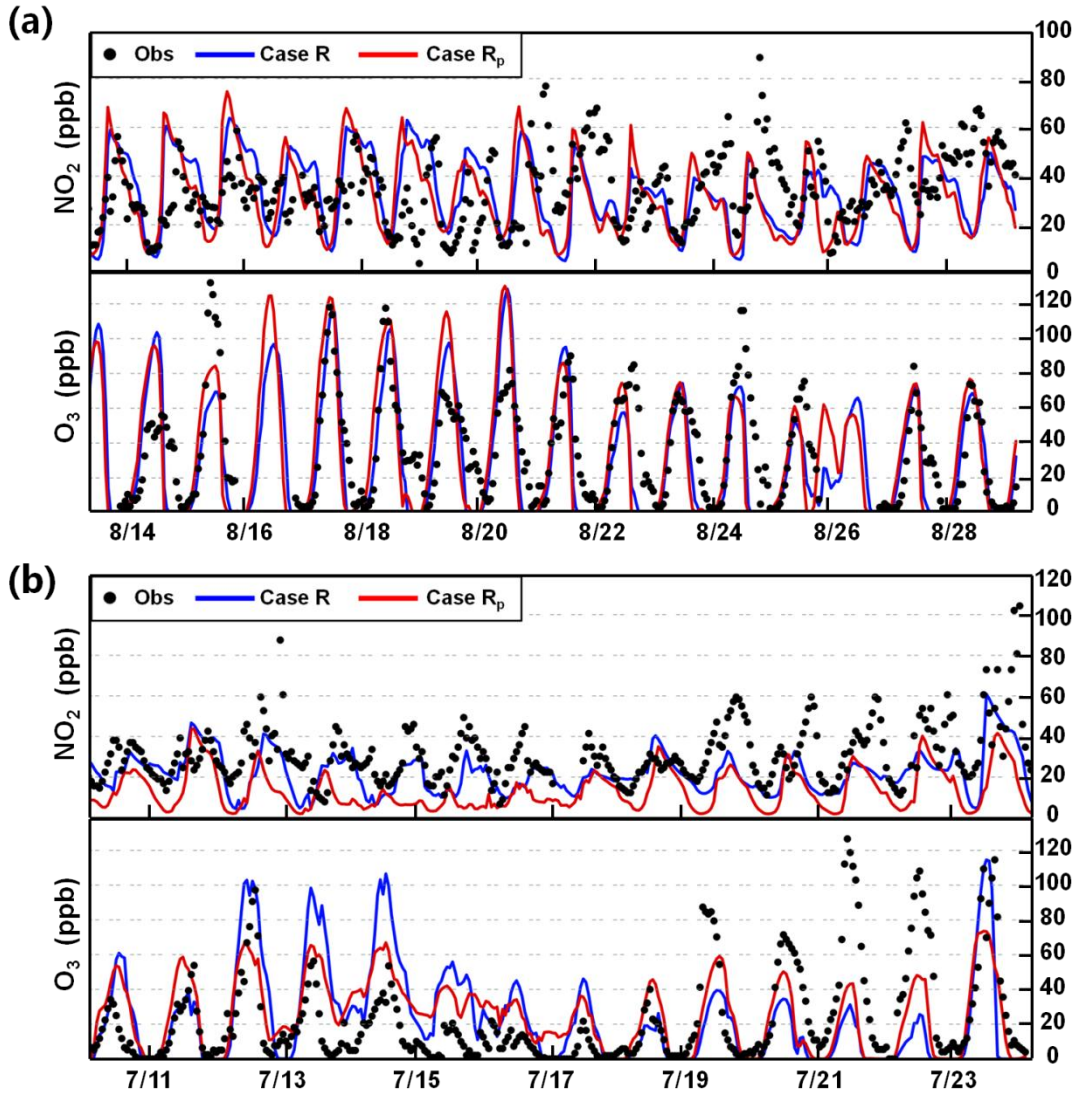

925
926 Fig. 4. Comparison of simulated and observed hourly-mean mixing ratios of NO_2 and
927 O_3 in (a) Beijing on 14–28 August 2007 and (b) Guangzhou on 11–23 July 2006.

928

929

930

931

932

933

934

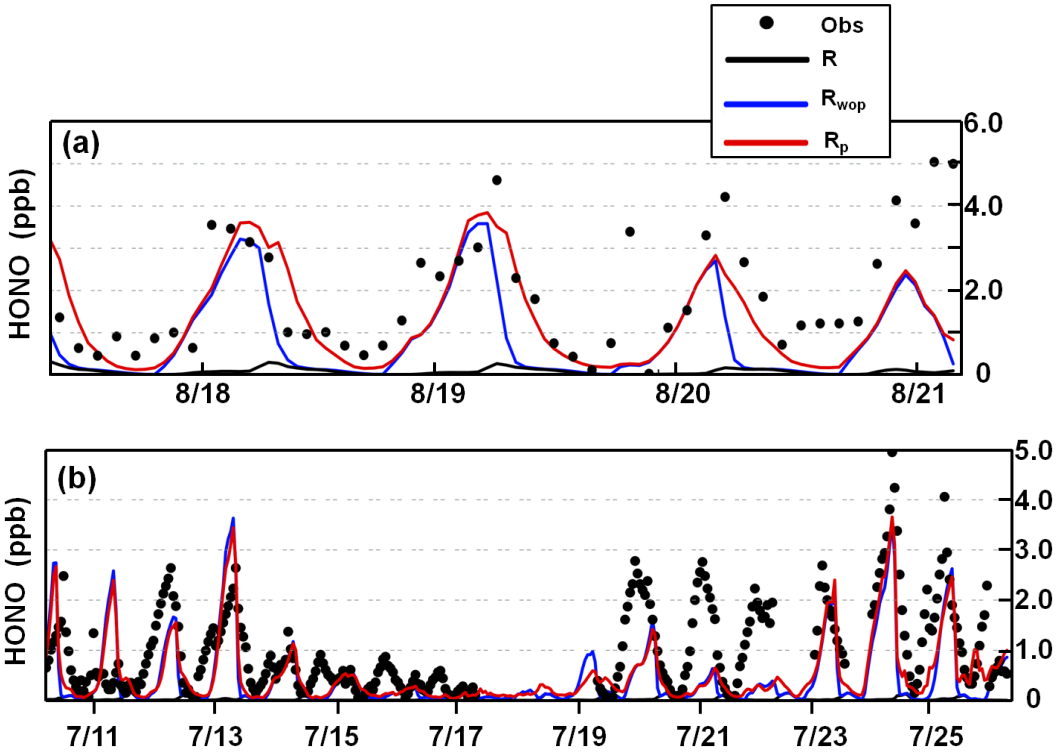

Fig. 5. Comparison of simulated and observed hourly-mean HONO mixing ratios at the Peking University site in (a) Beijing on 17–20 August 2007 (Spataro et al., 2013) and (b) the Backgarden site in Guangzhou on 11–25 July 2006 (X. Li et al., 2012).

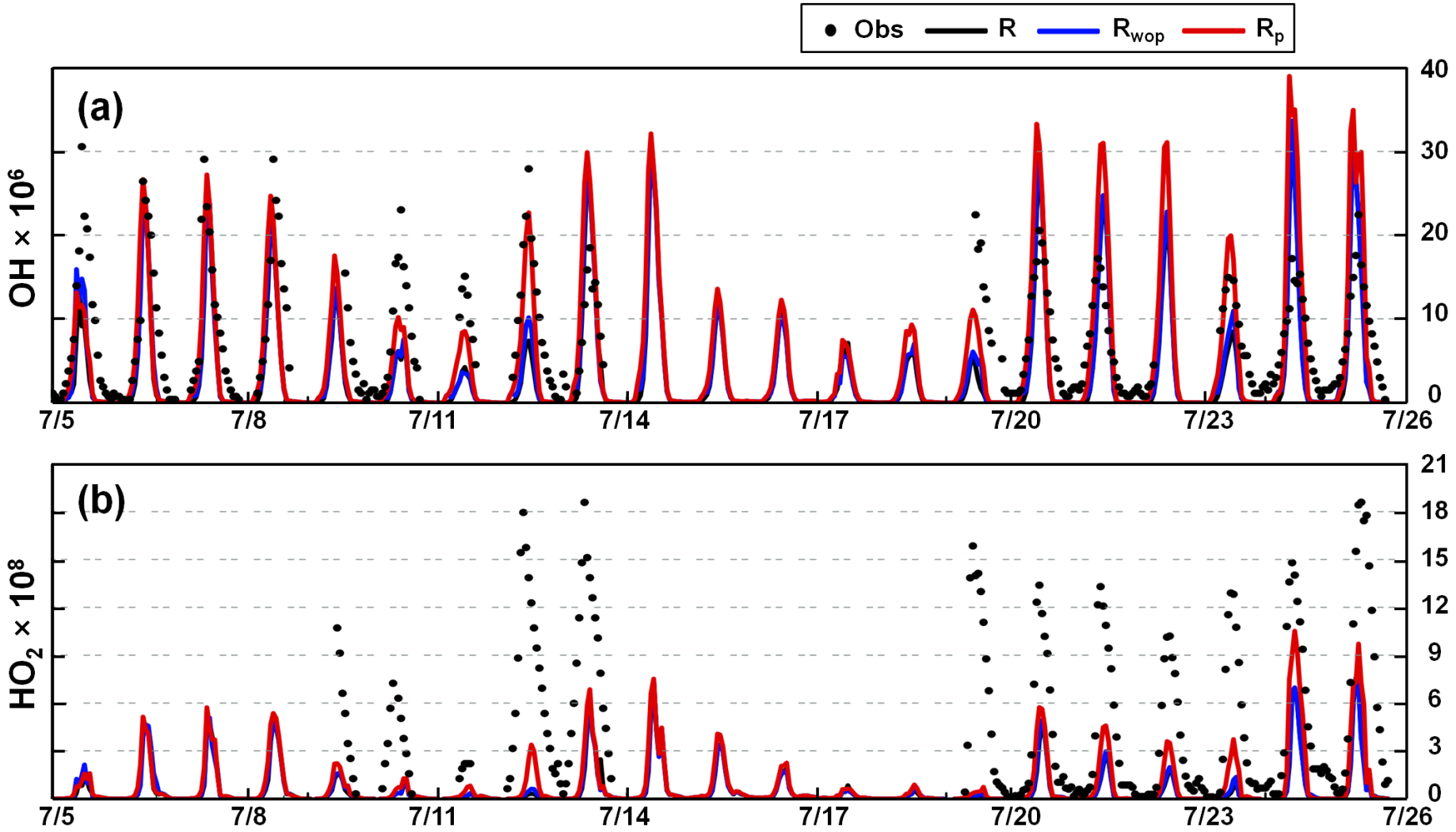

Fig. 6. Comparison of simulated and observed hourly-mean mixing ratios of OH and HO_2 at the Backgarden site in Guangzhou in July 2006 (Lu

et al., 2012).

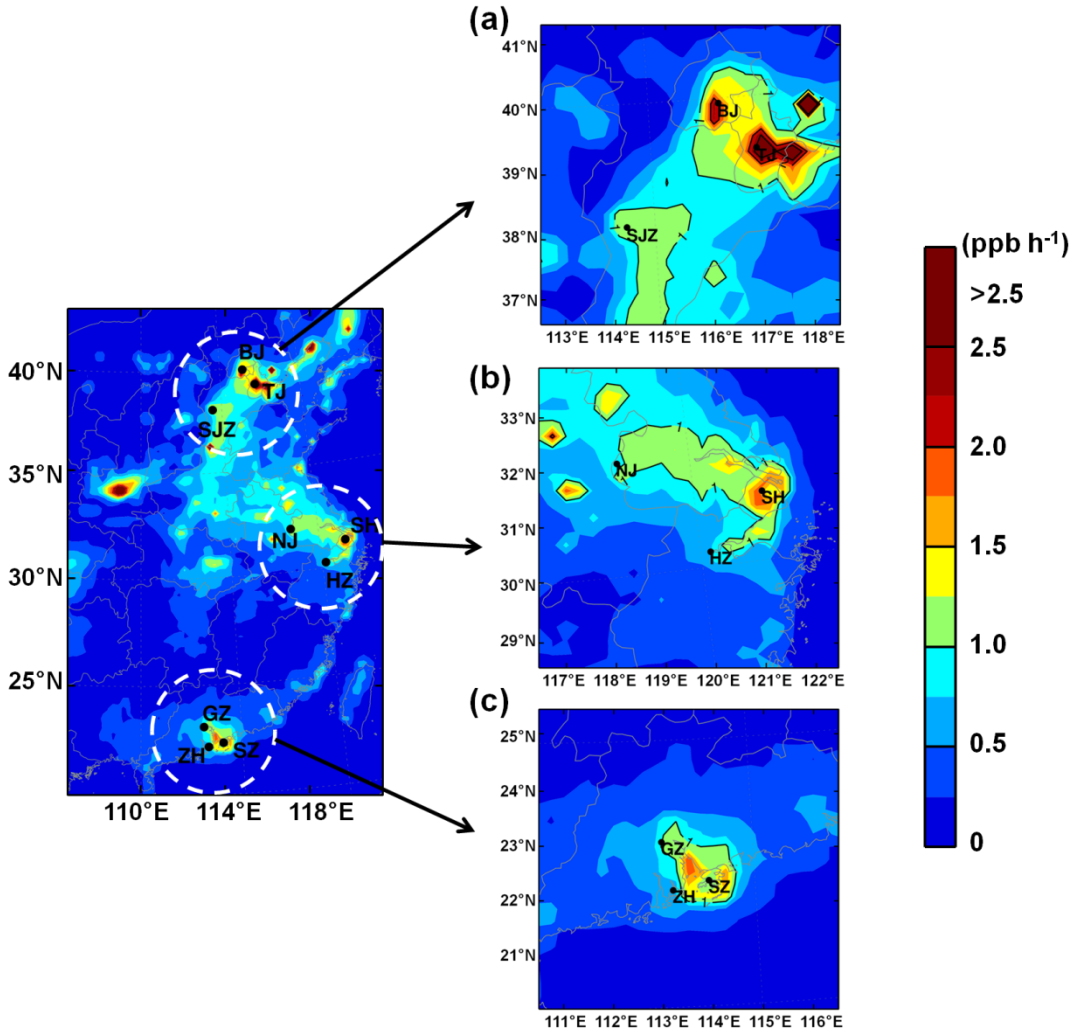

Fig. 7. Simulated unknown daytime HONO source (ppb h^{-1}) in the (a) BTH, (b) YRD, and (c) PRD regions in August 2007 (BJ, Beijing; TJ, Tianjin; SJZ, Shijiazhuang; SH, Shanghai; NJ, Nanjing; HZ, Hangzhou; GZ, Guangzhou; ZH, Zhuhai; SZ, Shenzhen).

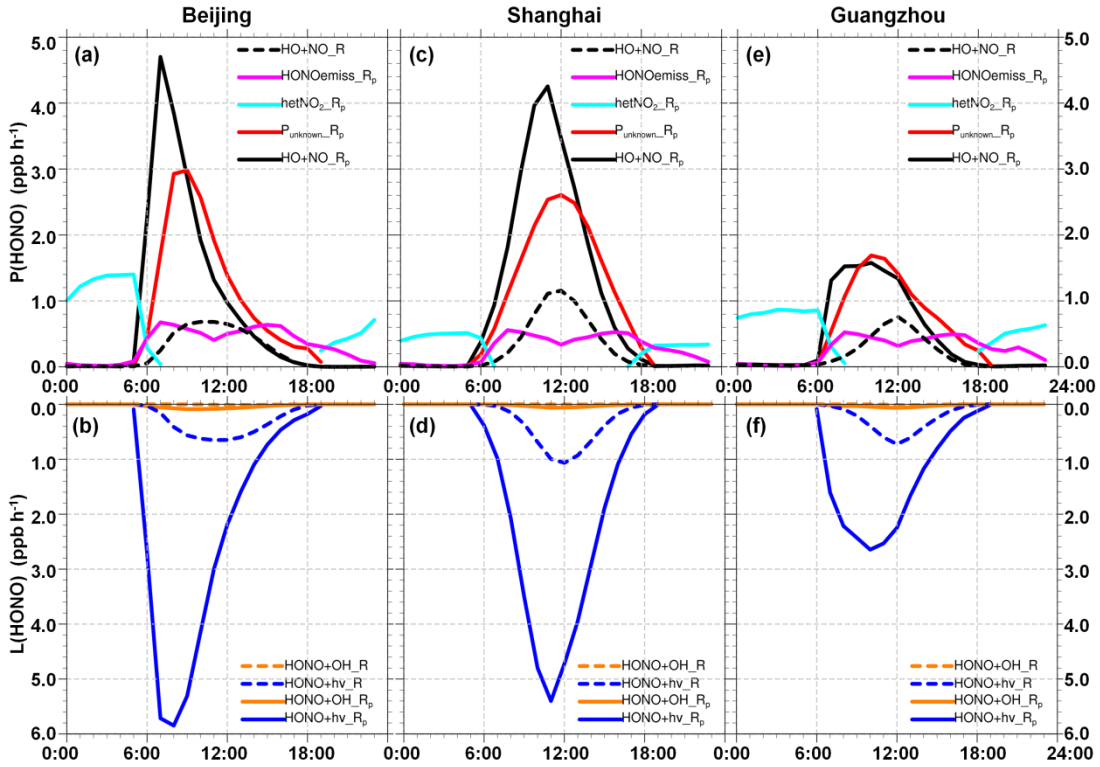

Fig. 8. Production [P(HONO)] and loss [L(HONO)] rates of HONO for cases R (dashed lines) and R_p (solid lines) in (a, b) Beijing, (c, d) Shanghai, and (e, f) Guangzhou in August 2007.

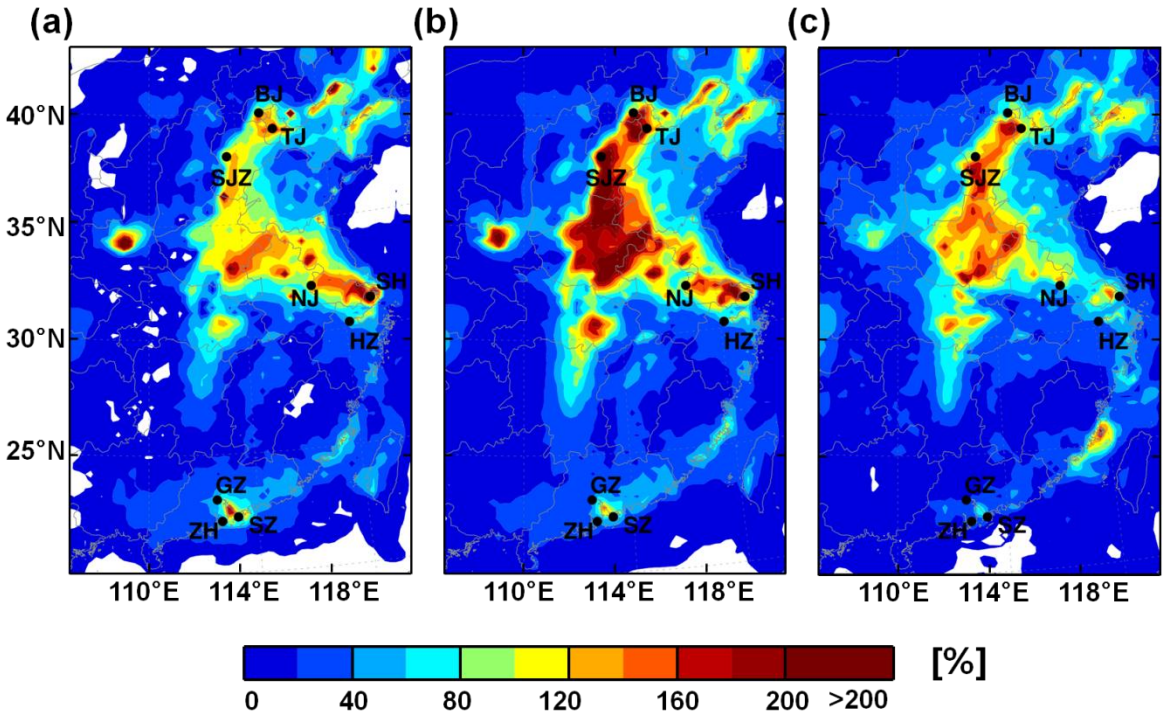

Fig. 9. Daytime (06:00–18:00 LST) percentage enhancements of (a) OH, (b) HO_2, and (c) RO_2 due to the unknown daytime HONO source (case R_p − case R_{wop}) in the coastal regions of China in August 2007.

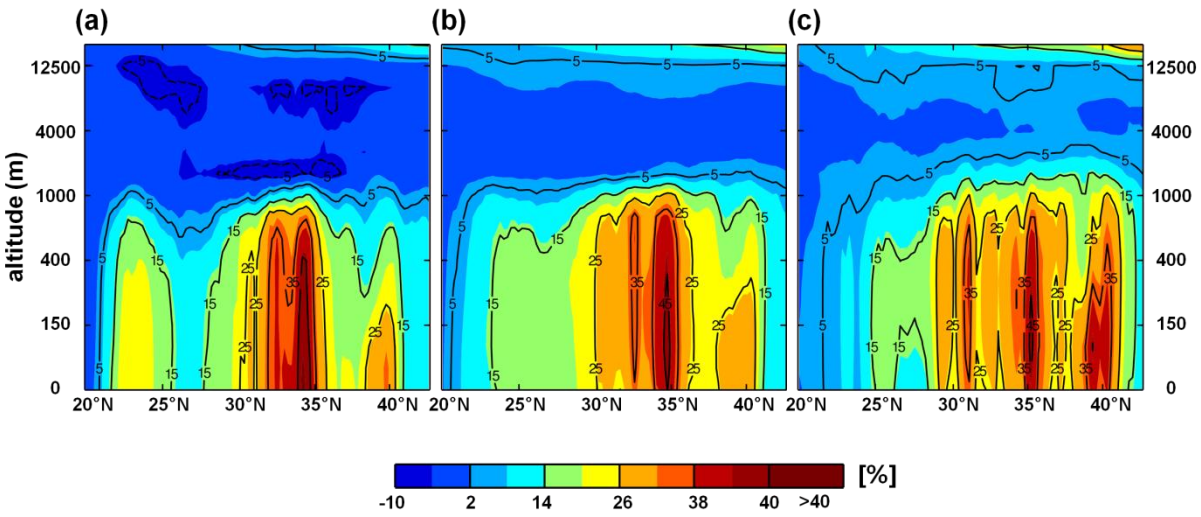

1014

1015 Fig. 10. Daytime (06:00–18:00 LST) meridional-mean percentage enhancements of (a)

1016 OH, (b) HO_2, and (c) RO_2 due to the unknown daytime HONO source (case R_p − case

1017 R_{wop}) in the coastal regions of China in August 2007.

1018

1019

1020

1021

1022

1023

1024

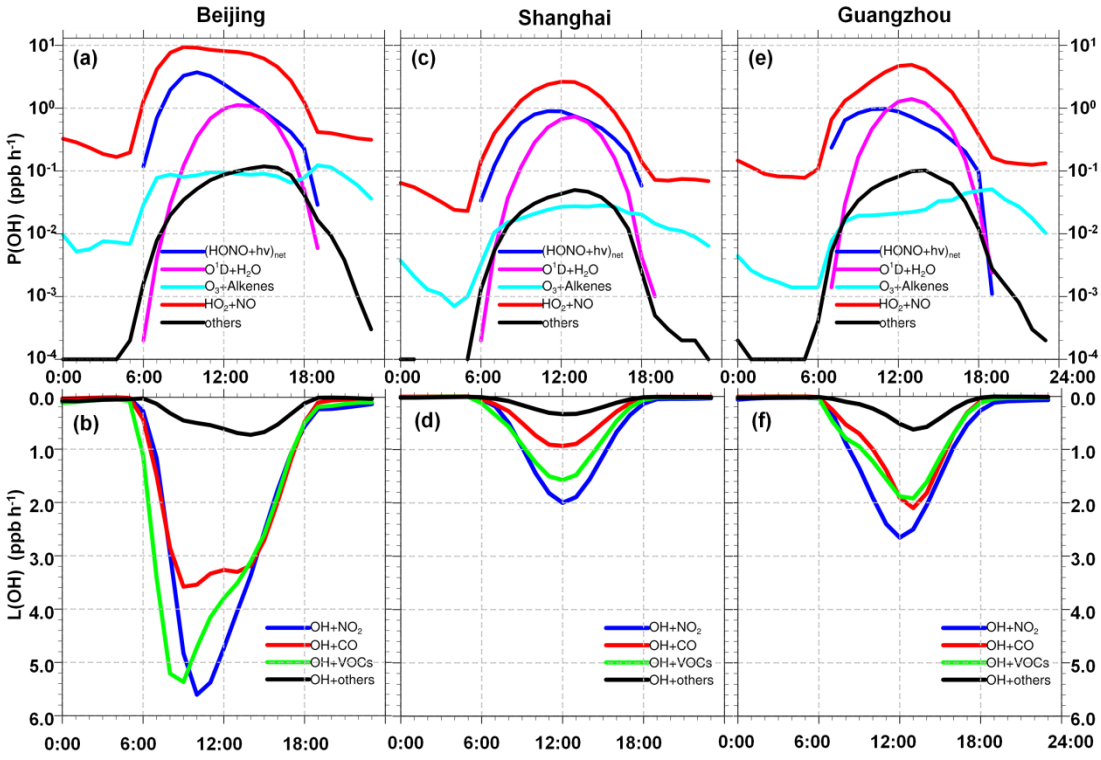

Fig. 11. Averaged production [P(OH)] and loss [L(OH)] rates of OH for case R_p in (a, b) Beijing, (c, d) Shanghai, and (e, f) Guangzhou in August 2007. $(HONO+hv)_{net}$ means the net OH production rate from HONO photolysis (subtracting OH + NO = HONO).

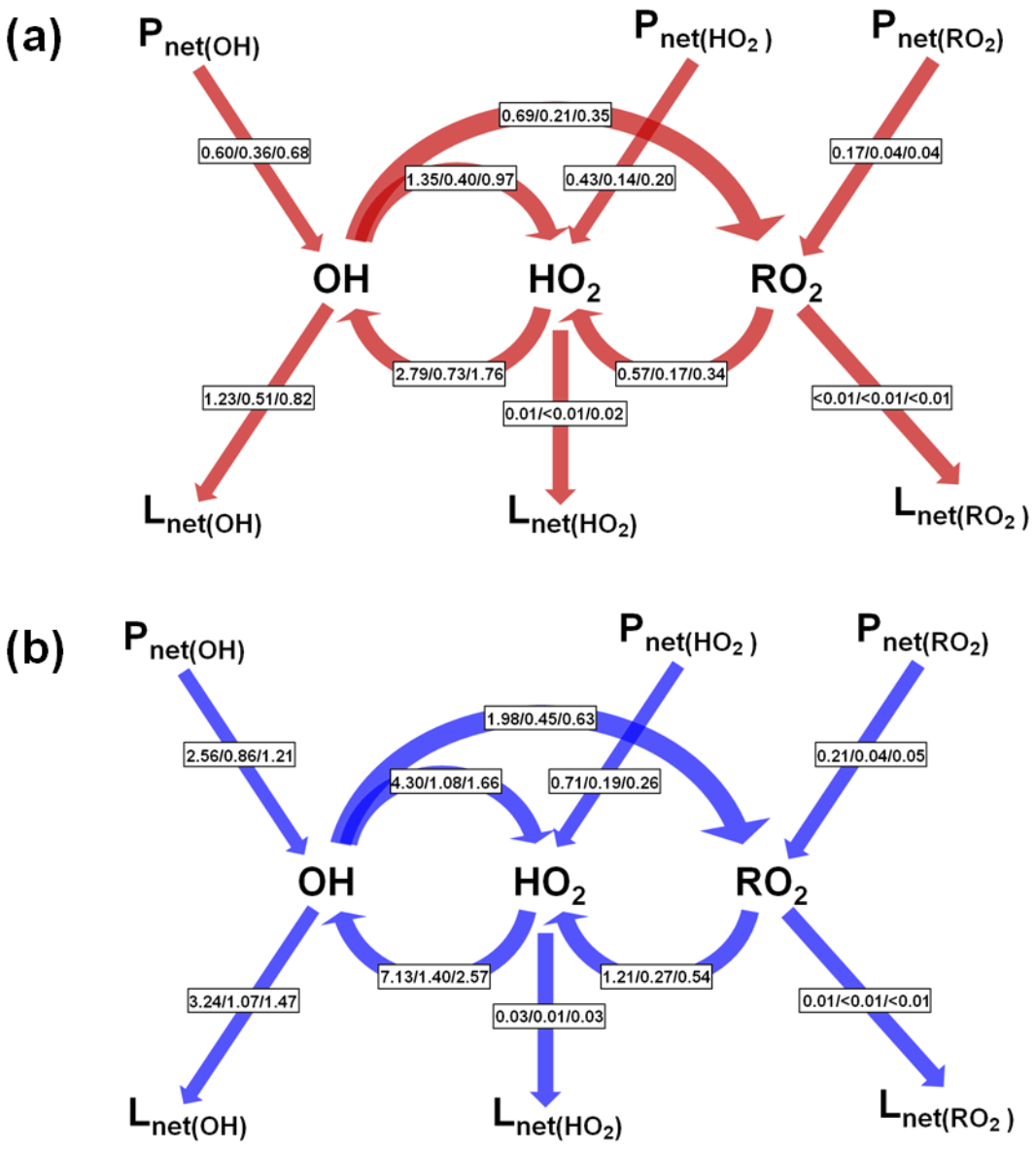

Fig. 12. Daytime (06:00–18:00 LST) average budgets of OH, HO_2 and RO_2 radicals (reaction rates, ppb h^{-1}) for cases (a) R and (b) R_p in Beijing/Shanghai/Guangzhou in August 2007.